

A Dynamic Model of the Cardiac Ventricular Action Potential

I. Simulations of Ionic Currents and Concentration Changes

Ching-Hsing Luo, Yoram Rudy

Abstract A mathematical model of the cardiac ventricular action potential is presented. In our previous work, the membrane Na^+ current and K^+ currents were formulated. The present article focuses on processes that regulate intracellular Ca^{2+} and depend on its concentration. The model presented here for the mammalian ventricular action potential is based mostly on the guinea pig ventricular cell. However, it provides the framework for modeling other types of ventricular cells with appropriate modifications made to account for species differences. The following processes are formulated: Ca^{2+} current through the L-type channel (I_{Ca}), the $\text{Na}^+/\text{Ca}^{2+}$ exchanger, Ca^{2+} release and uptake by the sarcoplasmic reticulum (SR), buffering of Ca^{2+} in the SR and in the myoplasm, a Ca^{2+} pump in the sarcolemma, the Na^+/K^+ pump, and a nonspecific Ca^{2+} -activated membrane current. Activation of I_{Ca} is an order of magnitude faster than in previous models.

Inactivation of I_{Ca} depends on both the membrane voltage and $[\text{Ca}^{2+}]_i$. SR is divided into two compartments, a network SR (NSR) and a junctional SR (JSR). Functionally, Ca^{2+} enters the NSR and translocates to the JSR following a monoexponential function. Release of Ca^{2+} occurs at JSR and can be triggered by two different mechanisms, Ca^{2+} -induced Ca^{2+} release and spontaneous release. The model provides the basis for the study of arrhythmogenic activity of the single myocyte including afterdepolarizations and triggered activity. It can simulate cellular responses under different degrees of Ca^{2+} overload. Such simulations are presented in our accompanying article in this issue of *Circulation Research*. (*Circ Res*. 1994;74:1071-1096.)

Key Words • cardiac action potential model • Ca^{2+} transients • sarcoplasmic reticulum • Ca^{2+} release

In 1991, we presented the first phase (referred to as the phase-1 L-R model) of a cardiac action potential model that was based on recent data from single-cell and single-channel preparations.¹ The earlier study focused on the depolarization and repolarization phases of the action potential and on phenomena that involve interaction between these processes. These included supernormal excitability, Wenckebach periodicity, and aperiodic responses of the cell to periodic stimulation. In terms of membrane ionic channel kinetics, the phase-1 model formulation concentrated on the fast Na^+ current (I_{Na}), the time-dependent K^+ current (I_K), the time-independent K^+ current (I_{K1}), and a plateau K^+ current (I_{Kp}). In that model, we introduced the dependence of the K^+ currents on $[\text{K}^+]_o$. However, the model did not account for dynamic changes in ionic concentrations and ionic fluxes during the action potential. In particular, intracellular Ca^{2+} transients could not be simulated because of the following limitations: (1) Ca^{2+} current through the L-type Ca^{2+} channel (I_{Ca}) was adopted from the model of Beeler and Reuter² (referred to as the B-R model). It was not reformulated to account for recent experimental findings regarding the channel kinetics, such as fast activation³ and inactivation that is both voltage and Ca^{2+} dependent.⁴⁻⁸ (2) The

phase-1 model included only ionic currents through gated channels in the sarcolemma but not other membrane processes (ie, pumps and exchangers) that contribute to changes in ionic concentrations. (3) Intracellular processes that dynamically regulate $[\text{Ca}^{2+}]_i$ (eg, Ca^{2+} uptake and release by the sarcoplasmic reticulum [SR]) were not incorporated in the phase-1 model.

In the phase-2 model presented here, I_{Ca} is reformulated on the basis of the most recent data from single-cell and single-channel experiments. Other processes that regulate the intracellular Ca^{2+} are also incorporated in the model. These include the following: the Na^+/K^+ pump (I_{NaK}), the $\text{Na}^+/\text{Ca}^{2+}$ exchanger (I_{NaCa}), a nonspecific Ca^{2+} -activated current ($I_{\text{ns(Ca)}}$), a Ca^{2+} pump in the sarcolemma ($I_{\text{p(Ca)}}$), buffering of Ca^{2+} ions in the myoplasm and in the SR, uptake of Ca^{2+} (I_{up}) by the network SR (NSR), translocation of Ca^{2+} (I_{tr}) from the NSR to junctional SR (JSR), leakage of Ca^{2+} (I_{leak}) from NSR, and release of Ca^{2+} ions (I_{rel}) by the JSR. A schematic diagram of the model is provided in Fig 1. The shaded areas indicate the presence of Ca^{2+} buffers. This model can simulate dynamic changes in ionic concentrations and, in particular, intracellular Ca^{2+} transients during the action potential. This property of the model could be the basis for future development of models of the excitation-contraction coupling process in cardiac myocytes.

In 1985, DiFrancesco and Noble⁹ published a model (D-N model) of the Purkinje action potential that incorporated many of the processes mentioned above. As we discussed previously,¹ certain properties of ionic channels were not fully represented in the D-N model because of the limited data from single-cell and single-

Received October 5, 1992; accepted February 7, 1994.

From the Department of Biomedical Engineering, Case Western Reserve University, Cleveland, Ohio.

Previously published in part in abstract form (*Circulation*. 1992;86[suppl I]:I-563).

Reprint requests to Prof Yoram Rudy, Department of Biomedical Engineering, Case Western Reserve University, Cleveland, OH 44106-7207.

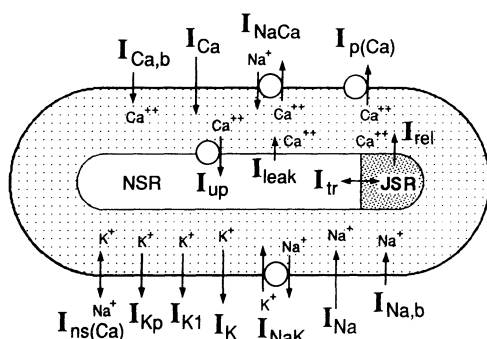


Fig 1. Schematic diagram of the cell model. The abbreviations representing ionic currents, pumps, and exchangers are defined in Appendix 2. The intracellular compartment is the sarcoplasmic reticulum (SR), which is divided into two subcompartments, the network SR (NSR) and the junctional SR (JSR). Dotted areas (in the myoplasm and the JSR) indicate presence of Ca^{2+} buffers.

channel experiments at the time. As a result, the D-N model could not simulate phenomena that were successfully simulated with our phase-1 model, such as Wenckebach periodicities in response to periodic stimulation. In addition, the D-N model did not take into account all processes that participate in the regulation of intracellular Ca^{2+} . One process that was not incorporated in the D-N model is buffering of Ca^{2+} by buffers in the myoplasm. As will be demonstrated by simulations in this article, this process is essential for a correct simulation of the intracellular Ca^{2+} transient and related phenomena. Another dynamic model of a cardiac action potential was developed for the frog atrial cell by Rasmusson et al.¹⁰ Although certain aspects of their model (in particular the kinetics of I_{Ca}) are similar to those of the model developed in the present study, other aspects are very different. A major difference is the lack of an SR and its role in the dynamics of intracellular Ca^{2+} in the Rasmusson model, reflecting the very small contribution of such processes in frog atrial cells.

In the present study, we provide a detailed description of the development and formulation of the various components of the model. We test each individual component by simulating physiological phenomena that involve this particular component. We then combine the individual processes into a complete model of the action potential and investigate the role played by the different components in generating the action potential. In our accompanying article in this issue of *Circulation Research*,¹¹ we use the model to study phenomena that are related to the excitation-contraction coupling process (eg, postextrasystolic mechanical potentiation), to Ca^{2+} -overload conditions, and to arrhythmogenic activity of the single cell (eg, early and delayed afterdepolarizations and triggered activity). The model could also provide the basis for future simulation studies of certain aspects of ischemia and of various interventions, the most important being the effects and mechanisms of action of channel blockers and other antiarrhythmic drugs.

In addition to the study of mechanisms that determine the behavior of the single cell, an accurate model of the action potential is important to simulation studies of propagation of excitation in cardiac tissue. Our studies of propagation^{12,13} and of reentry¹⁴ were limited by the inability to correctly simulate important aspects

of the action potential and situations of physiological and clinical importance (eg, Ca^{2+} overload and the effects of Ca^{2+} channel blockers). The need for a more complete model of the action potential to further elucidate mechanisms underlying abnormal propagation (eg, reentrant arrhythmias) provided yet another motivation for the work presented here.

Materials and Methods

General Approach

The general approach is based on a numerical reconstruction of the ventricular action potential using the following differential equation that describes the rate of change of membrane potential (V):

$$(1) \quad \frac{dV}{dt} = -(1/C_m)(I_i + I_{st})$$

where C_m is the membrane capacitance, I_{st} is a stimulus current, and I_i is the sum of all ionic currents through the membrane. In the model developed here, I_i includes ionic currents through voltage-gated channels and currents carried by other mechanisms (eg, I_{NaCa} and I_{NaK}). Gated channels are described by using Hodgkin-Huxley type formalism.¹⁵ This approach has been described in detail in the first phase of this work,¹ in which only gated channels were included in the model. In the same article,^{1(p1520)} we also discussed the correspondence between the ensemble behavior of ionic channels, as described by the Hodgkin-Huxley equations, and the single-channel behavior. The ionic currents are determined by ionic gates whose gating variables are obtained as a solution to a coupled system of differential equations. The integration algorithm¹ for solving the differential equations is based on the hybrid methods introduced by Rush and Larsen¹⁶ and Victorri et al.¹⁷ An adaptive nonlinear least-squares algorithm developed by Dennis et al¹⁸ is used for parameter estimation.

The model developed here accounts for dynamic changes of ionic concentrations during the action potential. The rate of change of ionic concentrations is given by

$$(2) \quad \frac{d[B]}{dt} = -(I_B \cdot A_{\text{Cap}})/(V_C \cdot z_B \cdot F)$$

where $[B]$ is the concentration of ion B, I_B is the sum of ionic currents carrying ion B, A_{Cap} is the capacitive membrane area, V_C is the volume of the compartment where $[B]$ is updated, z_B is the valence of ion B, and F is the Faraday constant.

All ionic currents are computed for 1 μF of cell membrane capacitance. Note that currents measured in single cells would be $\approx 10\,000$ times smaller than those reported here. Specific membrane capacity is set at 1 $\mu\text{F}/\text{cm}^2$.¹⁹ The formulation is based on experimental data adjusted to 37°C by use of the Q_{10} adjustment factor (defined in Appendix 2). For example, if I_{Ca} was 2 $\mu\text{A}/\mu\text{F}$ at 22°C with $Q_{10}=3$, then I_{Ca} at 37°C should be equal to $2 \cdot (Q_{10})^{(37-22)/10} = 10.39 \mu\text{A}/\mu\text{F}$. The complete set of equations for all ionic currents and other processes is provided in Appendix 1. Geometric parameters and standard ionic concentrations are also depicted in Appendix 1. Symbols used in the equations are defined in Appendix 2.

All computer programs were coded in FORTRAN 77 (Microsoft), and all simulations were implemented (double precision) on a Macintosh IIcx computer. The integration algorithm uses an adaptive time step that varies between 1 and 0.01 millisecond, and the potential is updated at steps that range from 0.2 to 1 mV. A time step < 0.01 millisecond is used if the potential step is > 1 mV (details are provided in Luo and Rudy¹). A detailed description of the formulation of the various components and their integration into the complete model of the action potential is provided in the following sections.

Formulation of the Model

Geometrical Considerations

The dimensions of the mammalian ventricular cell have been measured by several groups.²⁰⁻²⁵ On the basis of these

data, the shape of the cell in the model is represented as a circular cylinder 100 μm in length and 11 μm in radius. In ventricular cells, the large degree of membrane folding results in an actual surface area (represented by A_{Cap}) larger than that calculated from the cylindrical geometry (A_{Geo}). Assuming specific membrane capacity (C_s) of 1 $\mu\text{F}/\text{cm}^2$, Isenberg and Klöckner²⁰ found that the ratio (R_{CG}) of A_{Cap} (defined as C_m/C_s) to the geometric membrane area (A_{Geo}) is >2 . Values of R_{CG} measured by other groups^{21,22,25,26} are also close to, or smaller than, 2. Therefore, we set $R_{\text{CG}}=2$ in the model.

On the basis of measurements of Ca^{2+} -loading rate, drug effects, electron micrographs, and the density of its Ca^{2+} content, the SR appears to be functionally and structurally divided into two compartments: the JSR and the NSR.^{23,24,27-29} Functionally, Ca^{2+} ions enter the NSR from the myoplasm through an uptake process; they then translocate from the NSR into the JSR, where they are released into the myoplasm following the kinetics of the Ca^{2+} -induced Ca^{2+} release (CICR) process (Fabiano³⁰⁻³²) or the Ca^{2+} -overload triggering process.³³ On the basis of the measurements of Forbes et al²³ and those of other groups,^{34,35} we set the volume fraction of SR (F_{SR}) at 6% of the cell volume. The SR volume is divided into JSR (8%) and NSR (92%). Therefore, F_{JSR} is 0.48% = 8% · 6% and F_{NSR} is 5.52% = 92% · 6% of the cell volume. The mitochondria volume fraction (F_{mito}) is set at 26%.³⁶ The remaining volume ($F_{\text{myo}}=68\%$) is occupied by the myoplasm. For considerations of ion accumulation in extracellular clefts, $F_{\text{cell}} \cdot F_{\text{cleft}}$ is assumed to be 88% : 12%.^{24,34,35}

Standard Ionic Concentrations

The ionic concentrations are the same as those used in our previous model,¹ except for $[\text{Na}^+]_i$, which is decreased from 18 to 10 mmol/L. In the phase-1 model, the value $[\text{Na}^+]_i=18$ mmol/L was based on data measured at 22°C to 24°C.³⁷ However, other data suggest that $[\text{Na}^+]_i$ is smaller at 37°C. Sheu and Fozard³⁸ obtained Na^+ activity (a_{Na^+}) = 6.4 ± 1.2 mmol/L (equivalent to $[\text{Na}^+]_i=9.1 \pm 1.7$ mmol/L), Cannell et al³⁹ obtained $[\text{Na}^+]_i=8$ mmol/L, and Abete and Vassalle⁴⁰ obtained $a_{\text{Na}^+}=8$ mmol/L ($[\text{Na}^+]_i=11.4$ mmol/L) at 37°C. An overestimation of $[\text{Na}^+]$ acts to depress the capability of I_{NaCa} to extrude Ca^{2+} ions out of the cell. On the basis of the 37°C data and to maintain normal exchanger activity, we set $[\text{Na}^+]_i=10$ mmol/L. The resting $[\text{Ca}^{2+}]_i$ is set at 0.12 $\mu\text{mol}/\text{L}$ on the basis of the measured values of 0.136 ± 0.026 $\mu\text{mol}/\text{L}$ by Takamatsu and Wier⁴¹ and ≈0.12 $\mu\text{mol}/\text{L}$ by Beuckelmann and Wier.⁴²

Ionic Currents in the Sarcolemma

I_{Na} , the fast Na^+ current. The formulation of I_{Na} in the phase-2 model is the same as that in the phase-1 model,¹ except that the maximum conductance (\bar{G}_{Na}) is decreased from 23 to 16 millisiemens/ μF to compensate for the increased reversal potential (E_{Na} , from 54.4 to 70 mV) due to the lower $[\text{Na}^+]_i$ (10 instead of 18 mmol/L). Without this adjustment of \bar{G}_{Na} , the computed peak inward current is too large for ventricular cells (>450 $\mu\text{A}/\mu\text{F}$). For $\bar{G}_{\text{Na}}=16$ millisiemens/ μF , an acceptable value (380 $\mu\text{A}/\mu\text{F}$) is obtained, close to 400 $\mu\text{A}/\mu\text{F}$ in the phase-1 model. Note that this value of $\bar{G}_{\text{Na}}=16$ millisiemens/ μF is in the range of measured Na^+ conductances.⁴³ It should be noted that the equation for α_m (Appendix 1) is slightly modified from that given in Ebihara and Johnson (E-J)⁴⁴; an error in sign in the original E-J article is corrected, and a factor of 0.1 is introduced to provide a realistic activation threshold of I_{Na} (-58.8 mV) in a mammalian ventricular cell. These adjustments to the E-J formulation were first introduced in the phase-1 model.¹

Ionic currents through the L-type Ca^{2+} channel. The L-type channel is permeable to Ca^{2+} , Na^+ , and K^+ , with a permeability ratio of 2800 : 3.5 : 1, respectively.^{5,7,8,45} The total current through this channel is expressed as the sum of the individual component currents: $I_{\text{Ca,t}}=I_{\text{Ca}}+I_{\text{Ca,K}}+I_{\text{Ca,Na}}$ (see Appendix 2 for

definitions). Note that in view of the much larger permeability to Ca^{2+} , the major contribution to $I_{\text{Ca,t}}$ is from I_{Ca} . As suggested by Campbell et al,⁴⁵ we formulate I_{Ca} by using the constant-field equation (Appendix 1). Similar kinetics are assumed for $I_{\text{Ca,K}}$ and $I_{\text{Ca,Na}}$, with the major difference being the much smaller permeabilities of these components. All the data measured at room temperature are adjusted to the physiological body temperature of 37°C, which is based on Q_{10} of 2.96 measured by Cavalie et al.⁴⁶ The maximum conductance of I_{Ca} is chosen as $\bar{G}_{\text{Ca}}=0.9$ millisiemens/ μF ,³ and the corresponding permeability is $P_{\text{Ca}}=5.4 \times 10^{-4}$ cm/s. Permeabilities of the other components are much smaller (Appendix 1) and satisfy the permeability ratio above.

Activation kinetics (d-gate). Because of the high series resistance and voltage inhomogeneities introduced by the tissue architecture (gap junctions, endothelium, intercellular cleft space), the activation kinetics of this channel could not be measured precisely in multicellular tissue preparations.³ In single-cell preparations, Isenberg and Klöckner³ were the first to measure the time constant of activation (τ_d), which was an order of magnitude faster than suggested by the previous measurements in tissue preparations. Our formulation of d (Appendix 1) follows that of Rasmusson et al¹⁰ and results in activation kinetics an order of magnitude faster than in the B-R model or in our phase-1 model.

Inactivation kinetics (f and f_{ca}). The inactivation process of I_{Ca} has been the subject of controversy since the 1980s. It has been characterized as purely voltage dependent (only f, Isenberg and Klöckner³), purely Ca^{2+} dependent (only f_{ca}),^{47,48} or as a combined voltage- and Ca^{2+} -dependent process ($f \cdot f_{\text{ca}}$).⁴⁻⁸ On the basis of recent experiments, the combined voltage- and Ca^{2+} -dependent kinetics is generally more accepted than the other two possibilities. This is because the voltage dependence of steady-state inactivation measured by the gapped double-pulse protocol⁸ cannot be explained by purely voltage-dependent kinetics. Therefore, we assume that the inactivation process is both, voltage and $[\text{Ca}^{2+}]_i$ dependent, and can be described in terms of a purely voltage-dependent gate f and a purely $[\text{Ca}^{2+}]_i$ -dependent gate f_{ca} . To measure the purely voltage-dependent kinetics (ie, f), Ca^{2+} is replaced by other ions that are not subject to Ca^{2+} -dependent inactivation. These include Ba^{2+} , Sr^{2+} , K^+ , and Na^+ .^{4,5,6,8,48-50} The use of these ions to measure the characteristics of f [ie, $f_{\text{s}}(V)$ and $\tau_f(V)$] has resulted in a variety of conflicting results.^{5,8,48,49} f_{s} is described as either partial-U-shaped^{48,49} or monotonically decreasing.⁸ τ_f is described as either bell-shaped^{5,8} or U-shaped.⁴⁹ This lack of consistency may be due to the differences in experimental conditions. Equations describing these different measurements are presented in Appendix 3. Note that in the equations the half-saturation potential and the slope factor are different from the values used by Rasmusson et al¹⁰ (32 and 8 mV instead of 35.06 and 8.6 mV). These changes were necessary for the simulated I_{Ca} inactivation process (in particular the inactivation parameter f_{s} ; see "Results") to be in the range of experimental measurements. In "Results," these different formulations and the formulation used in the D-N model⁹ are tested and compared in terms of their ability to simulate recent experiments in single ventricular cells under normal physiological conditions ($[\text{Ca}^{2+}]_o \geq 1.8$ mmol/L). On the basis of these simulations (described in "Results"), we identified the formulation in Appendix 1 as the best representation of the voltage-dependent inactivation process. This formulation was incorporated in the action potential model.

The kinetics of the Ca^{2+} -dependent inactivation were first formulated by Standen and Stanfield.⁴⁷ This formulation involved an unknown subsarcolemmal space and ionic diffusion from this space to the myoplasm. Such a small subsarcolemmal space would result in a high Ca^{2+} concentration in this layer and a strong Ca^{2+} dependence of inactivation. However, a high concentration of subsarcolemmal Ca^{2+} was not detected by

measurements of the $[Ca^{2+}]_i$ wave using a fura 2 imaging system.^{41,42} The measured intracellular $[Ca^{2+}]$ transient could be adequately interpreted on the basis of a single compartment (myoplasm). Therefore, we assume a single compartment and formulate the Ca^{2+} -dependent inactivation as follows: $f_{Ca} = 1/\{1 + ([Ca^{2+}]_i/K_{m,Ca})^2\}$, where $K_{m,Ca}$ ($= 0.6 \mu mol/L$) is the half-saturation concentration.

I_K , the time-dependent K^+ current. In the phase-1 L-R model,¹ we introduced a $[K^+]_o$ dependence of the I_K conductance ($\bar{G}_K \propto \sqrt{[K^+]_o}$) but retained the linear dependence of I_K on its activation parameter ($I_K \propto X$) as suggested by Beeler and Reuter² on the basis of experiments conducted in multicellular preparations. More recent experiments in single cells⁵¹ demonstrated an X^2 dependence of I_K (see equation in Appendix 1). We did not use this form in the phase-1 model because $I_K(X^2)$ as suggested by Matsuura et al⁵¹ failed to repolarize the membrane from plateau potentials to rest potential at low $[K^+]_o$. We¹ stated that this situation would have to be reexamined once a correct formulation of I_{Ca} was developed and incorporated in the model. In the phase-2 model presented here, a correct I_{Ca} is incorporated (see previous section). With this reformulated I_{Ca} , the situation is reversed, and $I_K(X^2)$ can repolarize the membrane to rest at all levels of $[K^+]_o$. The reasons for this different behavior will be explained in "Results." In the phase-2 model, we adopt the X^2 dependence, since this behavior was demonstrated in single cells.⁵¹

I_{K1} , the time-independent K^+ current. The formulation of this current is the same as in the phase-1 model, except for the value of the maximum conductance (\bar{G}_{K1}). \bar{G}_{K1} can be obtained from measurements by Sakmann and Trube⁵² and data from Isenberg and Klöckner.²⁰ At $[K^+]_o = 5.4 \text{ mmol/L}$ and $35^\circ C$, the whole-cell I_{K1} conductance is $\approx 150 \text{ nanosiemens}$,⁵² and the average capacitive membrane area is $2 \times 10^{-4} \text{ cm}^2$.²⁰ Therefore, average \bar{G}_{K1} is estimated at 0.75 millisiemens/ μF (note the $1 \mu F/\text{cm}^2$ specific membrane capacity). In the phase-1 model, the value $\bar{G}_{K1} = 0.6 \text{ millisiemens}/\mu F$ was used on the basis of the I_{K1} curve of the B-R model. The reason we did not use the calculated value of 0.75 millisiemens/ μF was that this value resulted in a plateau potential $< 0 \text{ mV}$ because of the incorrect formulation of I_{Ca} in the B-R model. Such a low level of plateau potential is not consistent with experimental measurements. In the phase-2 model, I_{Ca} is reformulated, and $\bar{G}_{K1} = 0.75 \text{ millisiemens}/\mu F$ is used.

I_{Kp} , the plateau K^+ current. This current is the same as in the phase-1 L-R model.

I_{NaCa} , the Na^+-Ca^{2+} exchanger. In mammalian cardiac cells, it is generally accepted that the exchanger stoichiometry $Na^+:Ca^{2+}$ is $3:1$ ^{42,53-56} and that K^+ ions are not cotransported by the exchanger.⁵⁷ The formulation of I_{NaCa} was first proposed by Mullins⁵⁸ and simplified by DiFrancesco and Noble.⁹ According to recent experiments,^{42,53,54} several properties were not represented correctly by the D-N model. These are as follows: $[Na^+]_o$ dependence, $[Ca^{2+}]_o$ dependence, and saturation of I_{NaCa} at very negative potentials. A formulation that can correctly duplicate these properties (see "Results") is listed in Appendix 1. In this equation, $\eta = 0.35^{42,53,59,60}$ is the position of the energy barrier that controls the voltage dependence of I_{NaCa} , and k_{sat} is the saturation factor that ensures saturation at very negative potentials.

I_{NaK} , the Na^+-K^+ pump. Under a wide range of normal and abnormal physiological conditions, the reversal potential of I_{NaK} is very negative ($\leq -200 \text{ mV}$).⁶¹ Therefore, our formulation of I_{NaK} does not consider backward operation of the pump. In the forward operation, the pump extrudes three Na^+ ions from the cell in exchange for two K^+ ions that enter the cell.⁶¹ A property of I_{NaK} that is not simulated correctly by the D-N model⁹ or by the model of Rasmusson et al¹⁰ is the voltage dependence of I_{NaK} at different levels of $[Na^+]_o$. This property has been measured by Nakao and Gadsby⁶² and Gadsby and Nakao.²⁵ The parameter values in Appendix 1 are based on measurements by several groups.^{25,62-70} The resting value of

I_{NaK} is $\approx 0.3 \mu A/\mu F$ for standard ionic concentrations. The value of K_{m,Na_i} (43.2 mmol/L) measured by Mogul et al⁶⁹ is much higher than values measured by others ($\approx 10 \text{ mmol/L}$). This high value of K_{m,Na_i} implies a maximum pump current (\bar{I}_{NaK}) as high as $10 \mu A/\mu F$ in order to predict correctly the pump current at the resting state.^{62,67,69,70} Such a high value of \bar{I}_{NaK} has never been reported. Therefore, $K_{m,Na_i} = 10 \text{ mmol/L}$ ⁶² is used in our model. Our formulation of I_{NaK} is provided in Appendix 1. This formulation correctly simulates the voltage dependence for all values of $[Na^+]_o$ (see "Results").

$I_{ns(Ca)}$, the nonspecific Ca^{2+} -activated current. This channel is suspected to conduct the arrhythmogenic transient inward current (I_{Ti}) under Ca^{2+} -overload conditions. This channel was not identified in single cardiac cells until Ehara et al⁷¹ presented their observations in guinea pig ventricular cells. The channel is equally permeable to Na^+ and K^+ ⁷¹ and much less permeable to Ca^{2+} .⁷² Therefore, $I_{ns(Ca)}$ is regarded as the sum of the Na^+ current ($I_{ns,Na}$) and the K^+ current ($I_{ns,K}$) through this channel. $I_{ns(Ca)}$ is formulated by using the constant-field equation together with a Ca^{2+} -activated term in which the Hill coefficient is equal to 3 (Appendix 1). The maximum conductance of this channel is estimated in the range of 7.2 to 72 nanosiemens for the total cell membrane,⁷¹ which is equivalent to a specific conductance of 0.036 to 0.36 millisiemens/ μF (assuming $C_m = 200 \text{ pF}$).³ The choice of the value $\bar{G}_{ns(Ca)} = 0.072 \text{ millisiemens}/\mu F$ (note that $1 \mu F$ implies a 1-cm^2 membrane area) is based on the data measured by Doerr et al⁷³ (see "Results"). The corresponding $P_{ns(Ca)}$ is $1.75 \times 10^{-7} \text{ cm/s}$.

$I_{p(Ca)}$, the sarcolemmal Ca^{2+} pump. This pump provides another mechanism, in addition to the exchanger (I_{NaCa}), for the extrusion of Ca^{2+} ions out of the cell. As suggested by Rasmusson et al,¹⁰ the pump is included in the model to maintain the low level of $[Ca^{2+}]_i$ at rest. $K_{m,p(Ca)} = 0.5 \mu mol/L$ is obtained from the measurements by Caroni et al.⁷⁴ Different values of $K_{m,p(Ca)}$ were used in other models.^{10,75,76}

$I_{Ca,b}$, the Ca^{2+} background current. $I_{Ca,b}$ is formulated as a linear leakage current. Its contribution to $[Ca^{2+}]_i$ is balanced by the Ca^{2+} ion extrusion through I_{NaCa} and $I_{p(Ca)}$ so that the resting level of $[Ca^{2+}]_i = 0.12 \mu mol/L$ is maintained.

$I_{Na,b}$, the Na^+ background current. $I_{Na,b}$ is also formulated as a linear leakage current. Its contribution to $[Na^+]_i$ is balanced by Na^+ ion extrusion through I_{NaK} and entry through I_{NaCa} so that the resting level of $[Na^+]_i$ is maintained.

I_V , the time-independent, purely voltage-dependent current. In the phase-1 L-R model, the total time-independent current, $I_{K1(T)}$, was expressed as a summation of I_{K1} , I_{Kp} , and I_b , where I_b was a K^+ background current.¹ In the phase-2 model, I_b is replaced by a summation of $I_{Na,b}$, $I_{Ca,b}$, $I_{p(Ca)}$, and I_{NaK} . Therefore, the total time-independent current is not a pure K^+ current. To clarify this situation, the notation of $I_{K1(T)}$ is changed to I_V , which denotes the total time-independent current, the sum of six ionic currents. The subscript V indicates that this current depends only on the membrane potential and not on time.

Ca^{2+} Buffers in the Myoplasm

The Ca^{2+} buffers are located in the internal sarcolemma and the myoplasm. In the sarcolemma, the buffer capacity ($> 1 \text{ mmol/L}$) is very large but may not play an important role in Ca^{2+} -buffering during the excitation-contraction coupling cycle.⁷⁷ In models of Ca^{2+} movement during muscle contraction,⁷⁸⁻⁸⁰ sarcolemmal buffers were neglected, and the Ca^{2+} ions released from the SR were only buffered in the myoplasm by calmodulin and troponin. We make similar assumptions in our model. The buffer concentrations listed in Appendix 1 were obtained from Wier and Yue,⁷⁹ and the buffering kinetics were from Robertson et al.⁷⁷ After the approach of Hilgemann and Noble,⁷⁵ we compute the steady-state buffering process numerically by using Steffensen's iterative method. The steady-state assumption is justified since it differs only slightly from the dynamic buffering process.

Ca²⁺ Fluxes in the SR

CICR by the JSR. The mechanism of Ca²⁺ release by the cardiac SR is known as the CICR process.³⁰⁻³² Following the suggestion of Backx et al,⁸⁰ we represented the release process in our model by assuming variable ([Ca²⁺]_i-dependent) release kinetics in combination with a fixed threshold for release. Since we are not considering [Ca²⁺]_i wave propagation,^{41,80} we represent the release process as if it occurred from a single JSR release site, ignoring spatial distribution of the JSR and the resulting [Ca²⁺]_i propagation.

Beuckelmann and Wier,⁴² in agreement with Fabiato,³⁰⁻³² found that the peak intracellular Ca²⁺ transient was proportional to the cumulative amount of Ca²⁺ ions that enters the cell within 10 milliseconds from the onset of stimulation, with almost no further increase due to Ca²⁺ entering the cell later than the first 10 milliseconds. This implies that the amount of Ca²⁺ released from the JSR depends on the amount of Ca²⁺ that enters the cell within 10 milliseconds from the onset of stimulation. In the model, we compute the increase in [Ca²⁺]_i 2 milliseconds (rather than 10 milliseconds) from the time of \dot{V}_{\max} and denote it as $\Delta[Ca^{2+}]_{i,2}$. This adjustment is made to account for the faster kinetics at 37°C (Beuckelmann and Wier's data are at 23°C). It is also consistent with the time of peak I_{Ca} (2 milliseconds, Fig 11B), when [Ca²⁺]_i-dependent inactivation of I_{Ca} is significant, implying a sufficiently large intracellular Ca²⁺ transient that requires JSR release as early as at 2 milliseconds. On the basis of the data of Beuckelmann and Wier,⁴² JSR release of Ca²⁺ ions is triggered at clamping potentials more positive than -30 mV. This potential threshold is equivalent to an increase of [Ca²⁺]_i by 0.18 μmol/L. Therefore, we define $\Delta[Ca^{2+}]_{i,th}=0.18 \mu mol/L$ as the threshold for JSR release. This value is in agreement with the measurements by Kawano et al.⁸¹ The complete formulation of I_{rel} due to CICR is provided in Appendix 1. The [Ca²⁺]_i-dependent term is multiplied by a two-exponential term with time constants for the activation (τ_{on}) and deactivation (τ_{off}) of the release process. The half-saturation concentration $K_{m,rel}=0.8 \mu mol/L$ was obtained from Chamberlain et al.⁸² $\tau_{on}=\tau_{off}=2$ milliseconds is set to ensure that the pulse-release is completed in 5 milliseconds.

Ca²⁺ release by the JSR under Ca²⁺-overload conditions. It is commonly found that spontaneous contractions occur in skinned cardiac cells,³⁰ in damaged tissues,⁸³ and in intact rat ventricular cells.⁸⁴ Normal CICR from the JSR requires external triggering ($\Delta[Ca^{2+}]_i$ in the myoplasm, outside the JSR). An alternative triggering process occurs from within the JSR under Ca²⁺-overload conditions. A simple heuristic model of spontaneous Ca²⁺ release from the JSR was proposed by Capogrossi et al⁸⁴ and Stern et al.³³ In this simple model, JSR releases all of its stored Ca²⁺ ions once the level of its releasable Ca²⁺ pool reaches a threshold, and then JSR-Ca²⁺ is replenished following a monoexponential time course. In our model, JSR is reloaded by Ca²⁺ ions from the NSR through a translocation process described by a simple monoexponential function. The threshold for internal triggering of Ca²⁺ release from the overloaded JSR depends on the species. The tendency for spontaneous Ca²⁺ release, in a decreasing order, is: rat > hamster > dog > cat > guinea pig > rabbit.³⁴ In normal rat ventricular cells at rest, spontaneous release can occur. Since most of the releasable Ca²⁺ in the JSR binds to the buffer calsequestrin (CSQN), we define the threshold in terms of percent [CSQN] that is Ca²⁺ bound. In rat ventricular cells at rest and under normal conditions (no Ca²⁺ overload), 68.5% of total [CSQN] binds with Ca²⁺ ions. In the model, we set the threshold for spontaneous release at [CSQN]_{th}=70% for the rat. For species other than the rat [CSQN]_{th} is >70%. The complete formulation of the spontaneous release process is provided in Appendix 1.

CSQN, the Ca²⁺ buffer in the JSR. The Ca²⁺ buffer CSQN increases the releasable pool of Ca²⁺ ions in the JSR. Otherwise, with such a small volume fraction of the cell

($F_{JSR}=0.48\%$), JSR cannot store sufficient Ca²⁺ ions to cause muscle contraction on release. The maximum value [CSQN]=31 mmol/L and the half-saturation concentration $K_{m,CSQN}=0.8 \mu mol/L$ were used by Cannell and Allen⁷⁸ in skeletal muscle simulations. It should be noted that the myoplasmic Ca²⁺-buffering capacity in skeletal muscle is much greater than in cardiac muscle; therefore, the value [CSQN]=10 mmol/L is used in our model to ensure that JSR is almost completely depleted of its Ca²⁺ contents during each excitation-contraction cycle and that the simulated peak intracellular Ca²⁺ transient is consistent with measured data. Similar to buffering in the myoplasm, we compute the buffering process in the JSR using Steffensen's iterative method assuming steady state.

I_{up} and I_{leak} , Ca²⁺ uptake and leakage by the NSR. Because of its small volume fraction (0.48%) and slow rate of Ca²⁺ uptake, Ca²⁺ uptake from the myoplasm by the JSR is negligible.²⁷ Therefore, in the model, direct uptake by the JSR is neglected, and Ca²⁺ ions enter the JSR only through the NSR by a translocation process. The kinetics of Ca²⁺ uptake from the myoplasm by the NSR can be described by the Michaelis-Menten equation (Haynes and Mandeno⁸⁵) shown in Appendix 1. On the basis of experimental findings^{85,86} and model simulations,^{79,80} maximum [Ca²⁺] in the NSR ([Ca²⁺]_{NSR}) is equal to 15 mmol/L, the Hill coefficient is 1, and half-saturation concentration ($K_{m,up}$) is 0.92 μmol/L. A maximum uptake rate (\bar{I}_{up}) faster than 0.003 mmol/L per millisecond is necessary to reload into the NSR all the Ca²⁺ ions that were released from the JSR during an action potential.³² Therefore, $\bar{I}_{up}=0.005 \text{ mmol/L per millisecond}$ was chosen in the model. The net rate of Ca²⁺ uptake into the NSR is the difference between I_{up} and I_{leak} , where $I_{leak}=K_{leak} \cdot [Ca^{2+}]_{NSR}$. To obtain $[Ca^{2+}]_{NSR}=15 \text{ mmol/L}$, the leakage rate of Ca²⁺ out of the NSR (K_{leak}) is set equal to $\bar{I}_{up}/[Ca^{2+}]_{NSR}=0.000333 \text{ ms}^{-1}$.

I_{tr} , translocation of Ca²⁺ ions from the NSR to the JSR. The kinetics of Ca²⁺ translocation from the uptake store (NSR) to the release store (JSR) was elucidated by investigating force-interval relations such as postextrasystolic restitution and potentiation.^{79,87} Both relations can be described by monoexponential functions with the same time constant.⁸⁷ On the basis of the data ($\tau_{tr}=182 \pm 44$ milliseconds or $\tau_{tr}=176 \pm 18$ milliseconds) measured by Yue et al,⁸⁷ $\tau_{tr}=180$ milliseconds is chosen for the time constant in the model. The complete equation for I_{tr} is provided in Appendix 1.

Results

The "Results" section is divided into two parts. The first set of simulations (Figs 2 through 12) deals with properties of the individual components of the model. In particular, we evaluate the representation of each component by simulating relevant experimental protocols and comparing the simulated results with published experimental findings. We also use the simulations to answer important questions related to the characteristics and mechanisms of the various component processes. Since I_{Na} , I_{K1} , and I_{Kp} are the same as in the phase-1 model, they are not discussed here. The second set of simulations (Figs 13 through 19) deals with the integration of the various components into a complete model of the action potential and investigates the role and contribution of each component at different phases of the action potential.

Physiological Behavior of Various Components of the Model

Voltage-Dependent Inactivation of I_{Ca}

The inactivation process of I_{Ca} is both voltage and Ca²⁺ dependent and can be formulated as $f \cdot f_{Ca}$, where

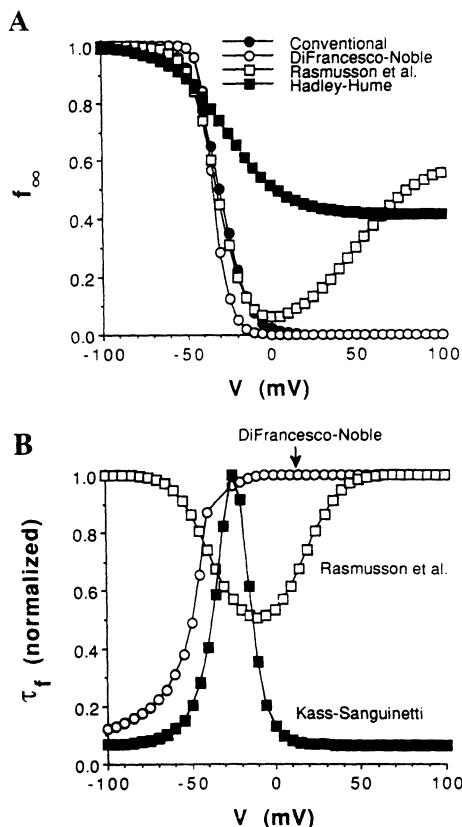


Fig 2. Graphs showing different formulations of the inactivation gate of the L-type Ca^{2+} channel (f-gate). A shows steady-state inactivation (f_z); B, the time constant (τ_f). Note that τ_f is normalized to its maximum value. The maximum τ_f is 20 milliseconds for DiFrancesco and Noble,⁹ 50 milliseconds for Rasmusson et al.,¹⁰ and 253.2 milliseconds for Kass and Sanguinetti.⁵ V indicates membrane potential. Data for Hadley and Hume are presented in Reference 8. Equations are provided in Appendix 3.

f is a purely voltage-dependent gate and f_{ca} depends only on the concentration of free Ca^{2+} ions in the myoplasm, $[\text{Ca}^{2+}]_i$. As mentioned in "Materials and Methods," several conflicting measurements and different formulations of the f-gate exist in the literature.^{5,8,48,49} Steady-state inactivation (f_z) and the time constant (τ_f) from several studies are plotted in Fig 2A and 2B, respectively, for the range of membrane potentials from -100 to $+100$ mV. Corresponding equations are provided in Appendix 3. f_z and τ_f , measured by Campbell et al⁴⁹ and formulated by Rasmusson et al,¹⁰ are partially U-shaped (f_z , Fig 2A) and fully U-shaped (τ_f , Fig 2B). f_z and τ_f , measured by Kass and Sanguinetti⁵ and Hadley and Hume,⁸ are monotonically decreasing to a nonzero value (f_z , Fig 2A) and are bell-shaped (τ_f , Fig 2B). All of these parameters were obtained by using the gapped double-pulse protocol (see below). In contrast, f_z in the D-N model is based on measurements using the conventional double-step protocol (described below) and is monotonically decreasing to zero (Fig 2A). τ_f in the D-N model is monotonically increasing to the value of 20 milliseconds (normalized to 1 in Fig 2B). For a more complete comparison of possible formulations, we add another set (f_z and τ_f), where f_z is monotonically decreasing to zero (our fit to the conventional double-step data, Fig 2A) and τ_f is bell-shaped (Kass-Sanguinetti, Fig 2B). In the following

simulations, we use these four different formulations of f in an attempt to reconcile the differences between them and to relate them to the different experimental protocols used for their measurements. In all simulations (except the D-N model), f_{ca} of Appendix 1 was used. Simulations involving the D-N model used the D-N formulation as depicted in Appendix 3. Protocols 1 and 2 below follow the experimental protocols of Campbell et al.⁴⁹

Protocol 1: $f_z(c)$, steady-state inactivation measured by the conventional double-step protocol. The protocol is as follows: membrane potential is first stepped from -60 mV to various potentials for 1000 milliseconds and then (second step) to 10 mV for 100 milliseconds and finally clamped back to the holding potential of -60 mV. From the peak inward current obtained at the second step, one subtracts the minimum current at the end of this step. This difference peak inward current (called the "visual estimate" current by Isenberg and Klöckner³) is normalized by its maximum value and plotted as a function of the different potentials of the first step. The resulting steady-state inactivation curve reflects the combined voltage- and Ca^{2+} -dependent processes (f_z and f_{ca} , respectively) and is denoted as $f_z(c)$ to differentiate it from $f_z(g)$, measured by the gapped double-pulse protocol (see below). We simulate this protocol by using our model (L-R) with the conventional f_z and τ_f of Kass and Sanguinetti,⁵ with f_z of Hadley and Hume⁸ and τ_f of Kass and Sanguinetti, and with f of Rasmusson et al.¹⁰ In addition, the D-N model is used for the simulation. $f_z(c)$ obtained by using the different models is quite similar and is adequately described by the conventional Boltzmann equation $f_z = 1/[1 + \exp((V - V_h)/K)]$ with different values of slope factor (K) and half-saturation potential (V_h). Parameter values for the different models are as follows: $V_h = -35$ mV and $K = -8.26$ for the conventional f_z and τ_f of Kass and Sanguinetti, $V_h = -35$ mV and $K = -5.1$ mV for f_z of Hadley and Hume and τ_f of Kass and Sanguinetti, $V_h = -35$ mV and $K = -5.65$ mV for f of Rasmusson et al, and $V_h = -32.5$ mV and $K = -5.92$ mV for the D-N model. Note that these different values are all in the range of measurements.^{3,5,48,88,89} On the basis of these simulations, it is clear that the conventional double-step protocol cannot separate the four different models tested.

Protocol 2: $f_z(g)$, steady-state inactivation measured by the gapped double-pulse protocol. The protocol is shown in the inset of Fig 3A and is described in the legend. The peak inward current obtained at the second pulse is normalized by its maximum value and is plotted as a function of the different potentials of the first pulse. We denote the resulting inactivation parameter as $f_z(g)$. Two conditions are investigated in the simulations: (1) $[\text{Ca}^{2+}]_i = 0.12 \mu\text{mol/L}$ is fixed throughout the simulation (denoted as $[\text{Ca}^{2+}]_i$ -fixed in the figure); this condition eliminates the Ca^{2+} dependence of inactivation (f_{ca}), and only the voltage-dependence (f) is obtained. (2) $[\text{Ca}^{2+}]_i$ is free to change during the simulation (denoted as $[\text{Ca}^{2+}]_i$ -unclamped in the figure); this condition provides a measure of the steady-state inactivation as a product of f_{ca} and f . Simulation results obtained with the same four models as in the previous protocol are shown in Fig 3. As expected, $f_z(g)$ obtained under the $[\text{Ca}^{2+}]_i$ -fixed condition is about the same as the purely voltage-dependent f_z shown in Fig 2. Note that unlike

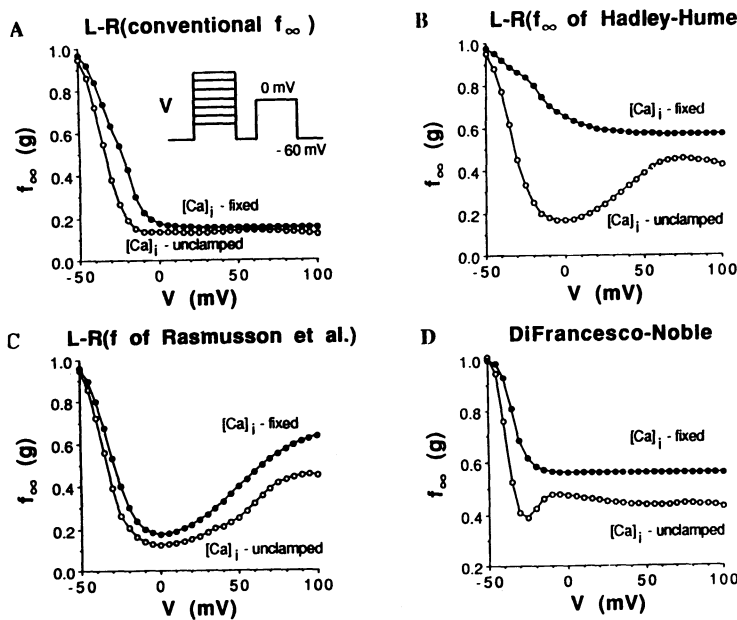


Fig 3. Graphs showing steady-state inactivation [$f_\infty(g)$] obtained by the gapped double-pulse protocol. A through D correspond to formulations 1 through 4 in Appendix 3. The protocol is shown in the inset of panel A; membrane is clamped to various potentials for 500 milliseconds (first pulse), and after a gap of 2 milliseconds at the holding potential (-60 mV), a second clamping pulse to 0 mV for 100 milliseconds is applied. Two conditions ($[Ca]_i$ -fixed and $[Ca]_i$ -unclamped) are investigated. The results indicate that only the formulations in panel B and panel C can duplicate the partial-U shape found experimentally. V indicates membrane potential; L-R, the Luo and Rudy model; and f and f_∞ , inactivation parameters. Data are taken from Hadley and Hume,⁸ Rasmusson et al.,¹⁰ and DiFrancesco and Noble.⁹

$f_\infty(c)$, $f_\infty(g)$ does not go to zero at positive potentials in Fig 3A and 3D. This is because at the onset of the second pulse, f is partially recovered from the fully inactivated state at the end of the first pulse (in the gapped protocol, the two pulses are separated by a gap of ≈ 2 milliseconds that permits partial recovery of f). In the range of positive potentials, f ($\approx f_\infty$) at the time of peak inward current at the second pulse is ≈ 0.14 and 0.5 in panels A and D, respectively, of Fig 3. $f_\infty(g)$ obtained under the $[Ca]_i$ -unclamped condition is very different and reflects, in addition to voltage dependence, the effects of changes in $[Ca^{2+}]_i$. The models that adopt the conventional f_∞ (Fig 3A and the D-N model in Fig 3D) fail to duplicate the partial-U shape of the steady-state inactivation as obtained from the gapped double-pulse experiments.^{4,6,8,48,49} However, two of the models (Hadley and Hume,⁸ Fig 3B; Rasmusson et al.,¹⁰ Fig 3C) successfully simulate the partial-U shape. The difference between these two models is that the $[Ca^{2+}]_i$ -dependent component plays a much more important role in determining $f_\infty(g)$ in the Hadley and Hume model (compare panels B and C in Fig 3).

Reconstruction of the action potential. The previous simulations indicate that the Hadley and Hume⁸ and the Rasmusson et al.¹⁰ formulations of $f_\infty(g)$ cannot be easily distinguished and compared when using either the gapped double-pulse or the conventional double-step protocols. A further test procedure is to reconstruct the action potential by using these two different representations of f . These simulations are shown in Fig 4. Fig 4A depicts the experimental measurements of Doerr et al.⁷³ using the action-potential clamp technique. The experimental result (Fig 4A) is duplicated reasonably well by the model that adopts the f -gate of Rasmusson et al (Fig 4B). Note that both experiment (Fig 4A) and simulation (Fig 4B) show zero contribution of I_{Ca} to the action potential for $V \leq -35$ mV (arrows) during the repolarization phase, as mentioned in "Materials and Methods." In contrast, the action potential simulated using the formula of Hadley and Hume (Fig 4C) does not duplicate the experiment successfully. The action

potential duration (APD) is very long (≈ 415 milliseconds). This results from the following property of this model: when the membrane potential decreases gradually during the plateau phase, I_{Ca} increases (Fig 4C, bottom) because of the monotonic increase of f_∞ as the membrane potential repolarizes from $+40$ to -30 mV (Fig 2A). I_{Ca} continues to increase until the membrane potential is more negative than -20 mV. At this potential, I_{Ca} becomes largely inactivated because of the small value of the d -gate. This increasing inward (depolarizing) current during the plateau and repolarization

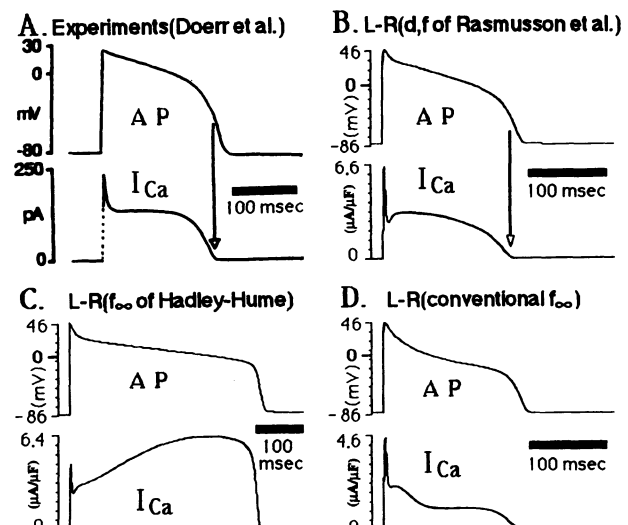


Fig 4. Tracings showing the behavior of the Ca^{2+} current (I_{Ca}) during an action potential (AP). A depicts the experimental results of Doerr et al.⁷³ I_{Ca} with activation parameter d and inactivation parameter f from Rasmusson et al.¹⁰ (panel B) duplicates well the experimental results (panel A). Note that the zero contribution of I_{Ca} at potentials more negative than -35 mV (arrow) is also duplicated in the model. Calibration bar in each panel is 100 milliseconds. Panels B, C, and D correspond to formulations 3, 2, and 1 in Appendix 3. Currents shown in the figures are for $1 \mu F$ of membrane capacitance. L-R indicates the Luo and Rudy model; f_∞ , steady-state inactivation parameter. Data are also from Hadley and Hume.⁸

phases acts to oppose the outward (repolarizing) I_K and prolongs the action potential. It is clear that the simulated I_{Ca} (Fig 4C, bottom) deviates greatly during the plateau and repolarization phases of an action potential from the experimental findings (Fig 4A, bottom). Note that in contrast to the increase of the Hadley and Hume f_z as the membrane potential repolarizes, f_z based on the Rasmusson et al formulation decreases monotonically as the membrane potential repolarizes from +50 to 0 mV and remains smaller than 0.2 down to -20 mV (Fig 2A). Of course, the conventional f_z (Fig 4D) cannot support a realistic value of I_{Ca} during the plateau because of its almost zero value at plateau potentials (Fig 2A). In conclusion, only the formulation of I_{Ca} inactivation suggested by Rasmusson et al can simulate successfully the conventional double-step protocol, the gapped double-pulse protocol, and I_{Ca} during the action potential. We adopt this formulation in our (L-R) model (Appendix 1) and use it in all of the simulations that follow.

Other Characteristics of I_{Ca}

The inactivation characteristics of I_{Ca} are complex, and their elucidation required several simulations, as described in the previous section. This section deals with other properties of I_{Ca} . Similar to the previous section, simulations are conducted and interpreted in relation to experimental findings.

Peak inward current and peak intracellular Ca^{2+} transient. The L-type channel is permeable to Ca^{2+} , K^+ , and Na^+ . The permeability ratio of $\text{Ca}^{2+}:\text{K}^+:\text{Na}^+$ is 2800:3.5:1. $I_{Ca,t}$ is the sum of the three ionic currents (I_{Ca} , $I_{Ca,K}$, and $I_{Ca,Na}$) through this channel. By clamping the membrane potential from -60 mV to various potentials for 100 milliseconds and then back to the holding potential of -60 mV, the peak inward currents of $I_{Ca,t}$ and its three individual components can be obtained. We have computed these currents as a function of membrane potential by simulating this protocol using our (L-R) model. $I_{Ca,t}$ and I_{Ca} almost overlap for $V \leq 35$ mV, and both display a bell-shaped behavior as a function of membrane potential (not shown). In the range of potentials from -50 to 90 mV, I_{Ca} is an inward current because the Nernst potential of the Ca^{2+} ions ($E_{Ca,N}$) = 127.5 mV and its maximum peak value is located at ≈ 0 mV; $I_{Ca,K}$ is an outward current; and $I_{Ca,Na}$ is an inward current for $V \leq E_{Na,N}$ (70 mV). The reversal potential (E_{Ca}) of the L-type channel is at $V = +56$ mV, where $I_{Ca,t}$ is zero. This value of E_{Ca} is the "apparent" reversal potential^{3,45} and can be computed by using the formula derived by Campbell et al.⁴⁵ One should note that the formula $I_{Ca} = G_{Ca} \cdot d \cdot f \cdot f_{Ca} \cdot (V - E_{Ca})$ represents the Ca^{2+} current only in the range of $V \leq 35$ mV, where $I_{Ca,t}$ and I_{Ca} almost overlap. For $V \geq 35$ mV, $I_{Ca,K}$ is significant and $I_{Ca,t}$ becomes an outward current for $V \geq 56$ mV, where $I_{Ca,K}$ is the major component current through the L-type channel. For comparison, we computed the peak inward currents using the D-N model. The behavior of these currents is similar to that in the L-R model, except that the reversal potential ($E_{Ca} = 75$ mV, instead of $E_{Ca} = 56$ mV in the L-R model) is very different and is not consistent with the value predicted by the constant-field equation.⁴⁵

As stated above, the peak amplitude of I_{Ca} as a function of the clamp potential is bell-shaped. If a larger peak inward current implies increased Ca^{2+} entry into the cell during the first 2 milliseconds after the onset of

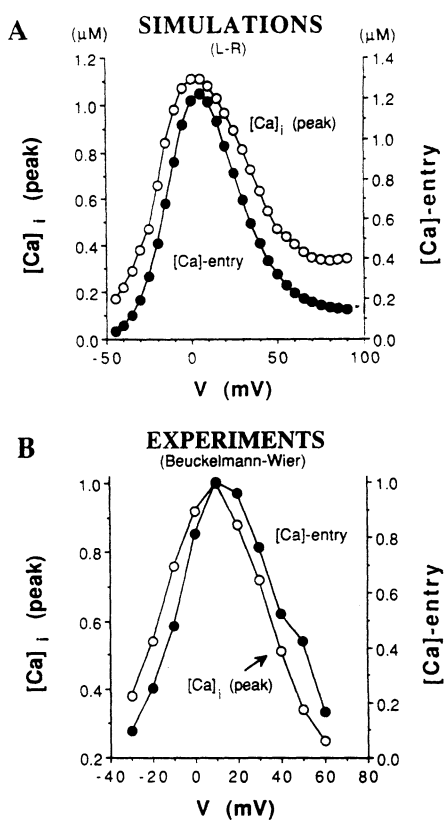


Fig 5. Graphs showing the relation between peak intracellular Ca^{2+} transient and Ca^{2+} entry. The protocol was to clamp the membrane potential from -60 mV to various potentials for 100 milliseconds and then back to the holding potential of -60 mV. As predicted by the kinetics of the Ca^{2+} -induced Ca^{2+} -release process, the peak intracellular Ca^{2+} transient is proportional to the cumulative Ca^{2+} entry 2 milliseconds from onset of stimulus in both the model simulations (A) and the experiments (B, Beuckelmann and Wier⁴²). L-R indicates the Luo and Rudy model; V, membrane potential. In panel B, $[Ca]_i$ (peak) and $[Ca]$ -entry are both normalized by their maximum values (the normalization causes an apparent crossover of the experimental curves).

depolarization, the amount of Ca^{2+} released from the JSR will also increase on the basis of the kinetics of the CICR process. This, in turn, will cause an increase of the peak intracellular Ca^{2+} transient. In Fig 5, both the Ca^{2+} entry during the first 2 milliseconds from the onset of stimulus and peak intracellular Ca^{2+} transient are shown to be bell-shaped (protocol is the same as that for obtaining the peak L-type currents above; see legend of Fig 5). Fig 5A shows the simulated results; Fig 5B shows the corresponding experimental data of Beuckelmann and Wier⁴² (their Fig 15A). The almost identical shape and near proportionality of the Ca^{2+} entry curve and the peak intracellular Ca^{2+} transient curve support the CICR hypothesis and proposed kinetics. The similarity of the Ca^{2+} entry curve (Fig 5) and the peak I_{Ca} bell-shaped curve (not shown) supports the hypothesis that a larger peak inward current results in a larger Ca^{2+} entry during the first 2 milliseconds. The similarity of the simulated curves (Fig 5A) and the experimental curves (Fig 5B) demonstrates that the kinetics of I_{Ca} and of the CICR process are represented accurately in our model.

Tail transients of $[Ca^{2+}]_i$. A "tail transient" is a transient increase in $[Ca^{2+}]_i$ elicited by repolarization. It

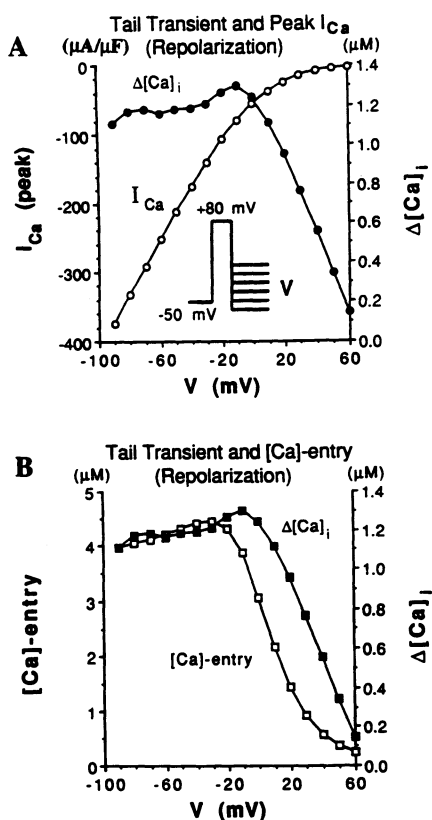


Fig 6. Graphs showing the relation between peak L-type Ca^{2+} current (I_{Ca}), cumulative Ca^{2+} entry at 2 milliseconds ([Ca]-entry), and tail transient ($\Delta[\text{Ca}]_i$). The protocol (inset) is to clamp the membrane potential from -50 to $+80$ mV for 20 milliseconds and then back to various repolarizing potentials. A shows that the tail transient does not follow the monotonic increase of the peak inward current. However, B shows that $\Delta[\text{Ca}]_i$ follows [Ca]-entry, in agreement with the proposed kinetics of the Ca^{2+} -induced Ca^{2+} -release process. Currents shown are for 1 μF of membrane capacitance. V indicates membrane potential.

is distinct from the intracellular Ca^{2+} transient during depolarization discussed in the preceding section. It is suggested that tail transients arise from SR Ca^{2+} release triggered by tails of the Ca^{2+} current.⁴² These tails occur when the driving force for Ca^{2+} influx is increased by repolarization and the Ca^{2+} conductance has not yet become deactivated. The dependence of tail transients on the repolarization voltage can be studied by using the protocol shown in the inset of Fig 6A and described in the legend. The tail transient is computed by subtracting the average $[\text{Ca}^{2+}]_i$ during depolarization from the peak $[\text{Ca}^{2+}]_i$ after onset of repolarization. Fig 6A shows the tail transient, $\Delta[\text{Ca}^{2+}]_i$, and the peak tail Ca^{2+} current, I_{Ca} , as a function of the repolarization voltage, V. Note that for repolarizing steps to membrane potentials more negative than -20 mV, the tail transient decreases while the (negative) magnitude of peak I_{Ca} increases. This behavior is in agreement with a similar experimental observation⁴² that $\Delta[\text{Ca}^{2+}]_i$ is not related directly to peak I_{Ca} for all values of V. In contrast, Fig 6B shows that the simulated tail transient is proportional to the cumulative Ca^{2+} entry 2 milliseconds after the onset of repolarization for all values of V. This proportionality is consistent with the CICR process and was observed experimentally as well.⁴² The lack of proportionality

between peak I_{Ca} and $\Delta[\text{Ca}^{2+}]_i$ (Fig 6A) and the proportionality between $\Delta[\text{Ca}^{2+}]_i$ and Ca^{2+} entry (Fig 6B) imply that peak I_{Ca} and Ca^{2+} entry are not proportional for all values of V. The reason that a larger peak inward Ca^{2+} current does not always result in a larger Ca^{2+} entry is the fast inactivation of I_{Ca} at potentials more negative than -20 mV. As the repolarization potential becomes more negative than -20 mV, the monotonic decrease of d_s and τ_d causes an early inactivation of I_{Ca} so that in spite of the large peak inward I_{Ca} , the total Ca^{2+} entry during the first 2 milliseconds is reduced. For instance, I_{Ca} for step repolarization to -90 mV attains a larger peak inward current (374 $\mu\text{A}/\mu\text{F}$ compared with 252 $\mu\text{A}/\mu\text{F}$) but inactivates much faster than I_{Ca} for step repolarization to -60 mV. As a result, the cumulative Ca^{2+} entry 2 milliseconds after the onset of repolarization is smaller for $V=-90$ mV ($[\text{Ca}^{2+}]$ entry = 3.96 $\mu\text{mol/L}$) than for $V=-60$ mV ($[\text{Ca}^{2+}]$ entry = 4.2 $\mu\text{mol/L}$).

Slow recovery from inactivation. The issue of slow recovery from inactivation of I_{Ca} was first discussed in 1974,⁴⁰ but its underlying mechanism is still not completely understood. This is because the values of the time constant of slow recovery from inactivation (τ_{rec}) are widely scattered. At $V=-50$ mV, Isenberg and Klöckner³ obtained $\tau_{rec}=45$ milliseconds. Two time constants of recovery were obtained by Josephson et al,⁴ $\tau_{rec}(\text{fast})=122$ milliseconds and $\tau_{rec}(\text{slow})=433$ milliseconds. Campbell et al⁴⁹ obtained the relation $\tau_{rec}=728 \cdot \exp(V/46.5)$ milliseconds, which differs from the data above. These inconsistencies complicate and limit the comparison between the simulation results and measured data.

In the model, I_{Ca} inactivation is formulated as a function not only of membrane potential but also of $[\text{Ca}^{2+}]_i$. As a result, the recovery of I_{Ca} is affected by the level of the intracellular Ca^{2+} transient during repolarization. During repolarization, I_{NaCa} is activated to pump Ca^{2+} ions out of the cell; therefore, the time course of the intracellular Ca^{2+} transient is determined by the pumping capacity of I_{NaCa} . In the range of membrane potentials from -100 to -30 mV, the time constant of the inactivation f-gate in the model is <50 milliseconds, whereas the time it takes for $[\text{Ca}^{2+}]_i$ to decrease from its peak value to its resting state value during repolarization is much longer than 50 milliseconds. Therefore, the recovery from inactivation of I_{Ca} in the model is controlled mostly by the time course of $[\text{Ca}^{2+}]_i$ and hence by the pumping capability of I_{NaCa} during repolarization.

The conventional protocol used to obtain τ_{rec} is shown in the inset of Fig 7 and is described in the legend. Based on our simulations, the relation $\tau_{rec}=355 \cdot \exp(V/109.5)$ is obtained and plotted in Fig 7. Compared with the experimental data at $V=-50$ mV, we obtained $\tau_{rec,\text{model}}=212.8$ milliseconds, much slower than the 45 milliseconds measured by Isenberg and Klöckner³ and the 122 milliseconds (fast) measured by Josephson et al.⁴ However, it is close to the 272 ± 31.9 milliseconds measured by Campbell et al⁴⁹ and smaller than the 433 milliseconds (slow) measured by Josephson et al.⁴

I_K , the Time-Dependent K^+ Current

As discussed in "Materials and Methods," I_K in the phase-2 model was reformulated on the basis of the study of Matsuura et al,⁵¹ who found that $I_K \propto X^2$ (rather than $I_K \propto X$, as proposed by Beeler and Reuter² and

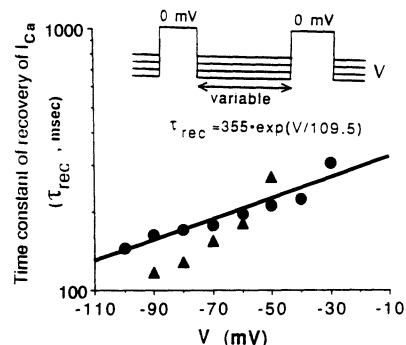


Fig 7. Time constant of recovery from inactivation of L-type Ca^{2+} current (I_{Ca}) as a function of membrane potential (V). The double-pulse recovery protocol is shown in the inset; for a fixed holding potential V (the membrane was held at this potential for 1 minute to ensure steady state), the interval between two clamping pulses (0 mV in amplitude and 100 milliseconds in duration) was varied from 40 to 1000 milliseconds to measure the recovery of I_{Ca} . The relation between the peak inward current measured at the second pulse and the interval between pulses fits a single exponential with a single time constant (τ_{rec}). By varying the holding potential, τ_{rec} is obtained from this (simulated) protocol for different values of V (black dots). The relation $\tau_{\text{rec}}=355 \cdot \exp(V/109.5)$ fits closely the dependence of τ_{rec} on V (solid line, note logarithmic scale). ● indicates simulation; ▲, experimental data of Campbell et al.⁴⁹

adopted in our phase-1 model). In the phase-1 model I_K of Matsuura et al could not repolarize the membrane from plateau to resting potential at low $[K^+]_o$. This situation is reexamined here, since other currents in the model, and in particular I_{Ca} , have been reformulated in the phase-2 model. We have simulated the action potential and the slow inward current (I_{si}) by using the phase-1 model (I_{si} is the same as in the B-R model) and the action potential and I_{Ca} using the phase-2 model. Both simulations are for low $[K^+]_o=2 \text{ mmol/L}$. I_{si} in the phase-1 simulation is still very large when the membrane potential repolarizes below -35 mV . This is inconsistent with the experimental findings⁷³ and results from the incorrect kinetics of the activation d-gate in the B-R model, in which d_z does not go to zero at potentials more negative than -35 mV . This significant nonzero inward current at $V \leq -35 \text{ mV}$ leads to an incorrect behavior.¹ For I_K of Matsuura et al, the value of the X -gate is very small at $V \leq -35 \text{ mV}$, and I_K is even smaller because of its X^2 dependence. Therefore, I_K of Matsuura et al fails to repolarize the membrane at this low $[K^+]_o$ (a condition that brings about a reduction in G_K) because of the significant opposing inward I_{si} at these potentials. In contrast, in the phase-2 model, I_{Ca} is zero for membrane potentials more negative than -35 mV , and I_K of Matsuura et al can adequately repolarize the membrane. Also, the simulated APDs for $[K^+]_o=2 \text{ mmol/L}$ are 540 and 325 milliseconds in the phase-1 and phase-2 models, respectively. Under conditions of $[K^+]_o=3.8 \text{ mmol/L}$ and $[Ca^{2+}]_o=3 \text{ mmol/L}$, Robinson et al⁹¹ obtained $APD=192 \pm 16 \text{ milliseconds}$ in isolated canine ventricular cells. For the same conditions, the APD computed by the phase-2 model is 205 milliseconds, very close to the measured APD. In contrast, the APD computed by the phase-1 model is unrealistically long (410 milliseconds) because of the unrealistically large contribution of I_{si} at $V \leq -35 \text{ mV}$ in this model.

Fig 8 depicts current-voltage curves of the fully

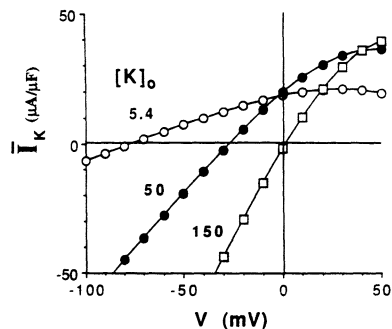


Fig 8. Current-voltage curves of the fully activated K^+ current (denoted I_K in the figure) for $[K^+]_o=5.4, 50$, and 150 mmol/L . Note significant crossover between curves of different values of $[K^+]_o$ and weak inward rectification. V indicates membrane potential. Currents shown in the figure are for $1 \mu\text{F}$ of membrane capacitance.

activated I_K ($\bar{I}_K=I_K/X^2$) for $[K^+]_o=5.4, 50$, and 150 mmol/L . The currents are simulated using the I_K formulation adopted in the present (phase-2) model, ie, $I_K \propto X^2$ as suggested by Matsuura et al⁵¹ (see Appendix 1). As a result, significant crossover between current-voltage curves at different values of $[K^+]_o$ is observed. This is different from the minimal crossover observed in the phase-1 model (Fig 11 of Luo and Rudy¹). Also, the degree of inward rectification of the inactivation I_K X_i -gate of Matsuura et al is ≈ 4.8 times smaller than that of the B-R model I_K , resulting in a fully activated outward I_K (\bar{I}_K , Matsuura et al), which is much larger than the B-R \bar{I}_K at positive potentials, enhancing its ability to repolarize the membrane at this potential range.

$I_{ns(Ca)}$, the Nonspecific Ca^{2+} -Activated Current

This current is equally permeable to K^+ and Na^+ and, therefore, is the sum of these two currents (ie, $I_{ns(Ca)}=I_{ns,K}+I_{ns,\text{Na}}$). In our model (simulation results are not shown), $I_{ns,K}$ displays outward rectification, whereas $I_{ns,\text{Na}}$ displays inward rectification. $I_{ns(Ca)}$, the sum of these two currents, appears as a linear leakage current with a reversal potential of $\approx 0 \text{ mV}$, as measured by Ehara et al.⁷¹ Under normal conditions (no Ca^{2+} overload, $P_{ns(Ca)}=1.75 \times 10^{-7}$, and $[Ca^{2+}]_i=0.12 \mu\text{mol/L}$), the maximum $I_{ns(Ca)}$ is $<0.008 \mu\text{A}/\mu\text{F}$ over the range of membrane potential from -100 to $+100 \text{ mV}$ (a negligible contribution). This current becomes significant, however, under conditions of Ca^{2+} overload.⁷³ In the model, for $[Ca^{2+}]_i=0.4 \mu\text{mol/L}$, $I_{ns(Ca)}$ reaches an amplitude of $4.4 \mu\text{A}/\mu\text{F}$.

The value of the maximum conductance, $\bar{G}_{ns(Ca)}$, estimated by Ehara et al,⁷¹ is in the wide range of 7.2 to 72 nanosiemens for the total cell membrane, which is equivalent to specific conductance in the range of 0.036 to 0.36 millisiemens/ μF . To decide on a specific value of $G_{ns(Ca)}$ within this range, we plotted the simulated action potential and compared it with the experimental results of Doerr et al⁷³ (their Fig 5). When $I_{ns(Ca)}$ is activated, an additional outward current is present at plateau potentials, and an additional inward current is present during the repolarization phase. As a result, plateau potentials are decreased, and the rate of repolarization is also decreased, resulting in a prolongation of the APD. With $\bar{G}_{ns(Ca)}=0.072 \text{ millisiemens}/\mu\text{F}$ (or $P_{ns(Ca)}=1.75 \times 10^{-7} \text{ cm}/$

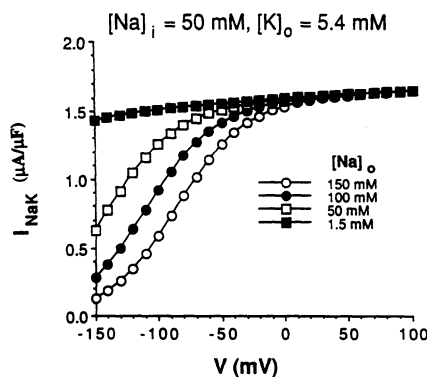


Fig 9. Graph showing the effects of changes in $[Na^+]$, on the voltage dependence of the Na^+ - K^+ pump (I_{NaK}). I_{NaK} depends strongly on membrane potential (V) for high $[Na^+]$. The dependence is decreased as $[Na^+]$ decreases. Also, for $V \geq 0$ mV, the dependence of I_{NaK} on membrane potential saturates regardless of the value of $[Na^+]$. These curves duplicate the experimental findings by Nakao and Gadsby.⁶² Currents shown in the figures are for 1 μ F of membrane capacitance.

s), the simulated behavior shown in Fig 13 duplicates accurately the experimental behavior obtained by Doerr et al⁷³ (their Fig 5). As stated above, for this value of $P_{ns(Ca)}$, the contribution of $I_{ns(Ca)}$ is practically negligible.

I_{NaK} , the Na^+ - K^+ Pump

The amplitude of I_{NaK} is a function of $[Na^+]_i$, $[K^+]_o$, $[Na^+]_o$, and the membrane potential.^{25,62} The dependence of I_{NaK} on $[Na^+]_i$ and $[K^+]_o$ is formulated by Hill equations, as depicted in Appendix 1. The dependence of I_{NaK} on the membrane potential is a function of $[Na^+]_o$. This property is simulated in Fig 9, which duplicates correctly the experimental findings of Nakao and Gadsby⁶² (their Fig 3). For the normal concentration of $[Na^+]_o = 140$ mmol/L, I_{NaK} depends strongly on the membrane potential, whereas at low values of $[Na^+]_o$, the dependence is decreased. At all values of $[Na^+]_o$, I_{NaK} saturates for membrane potential > 0 mV.

I_{NaCa} , the Na^+ - Ca^{2+} Exchanger

Fig 10A simulates the voltage dependence of I_{NaCa} for three different values of $[Na^+]_o$ in a $[Na^+]$ -free preparation, a situation that turns off the Ca^{2+} -influx mode of I_{NaCa} . Under these conditions, I_{NaCa} becomes an inward current (Ca^{2+} efflux and Na^+ influx with a stoichiometry of 1:3). The simulations (solid marks) duplicate well the experimental measurements (open marks) by Kimura et al⁵³ (their Fig 8B). In Fig 10B, three additional simulations (solid marks) are shown to duplicate the experiments (open marks) by Kimura et al⁵³ (their Fig 9A) and by Beuckelmann and Wier⁹² (B-W) (their Fig 6B). These include the voltage dependence of I_{NaCa} as a function of $[Ca^{2+}]_o$ and $[Ca^{2+}]_i$. $I_{NaCa}(V)$ is shown for $[Ca^{2+}]_o = 1$ mmol/L and $[Ca^{2+}]_i = 4$ mmol/L in a preparation of $[Na^+]_o = 140$ mmol/L, $[Na^+]_i = 10$ mmol/L, and $[Ca^{2+}]_i = 0.172$ μ mol/L (Fig 9A of Kimura et al⁵³). The B-W curve is for $[Ca^{2+}]_o = 2$ mmol/L, $[Ca^{2+}]_i = 0.45$ μ mol/L, $[Na^+]_o = 135$ mmol/L, and $[Na^+]_i = 15$ mmol/L. Note that the dependence of I_{NaCa} on $[Ca^{2+}]_o$ is duplicated well as $[Ca^{2+}]_o$ is changed from 1 to 4 mmol/L. A change in both $[Ca^{2+}]_o$ (from 1 and 4 mmol/L to 2 mmol/L in the B-W curve) and $[Ca^{2+}]_i$ (from 0.172 μ mol/L in the $[Ca^{2+}]_o = 1$ and 4 mmol/L curves to 0.45

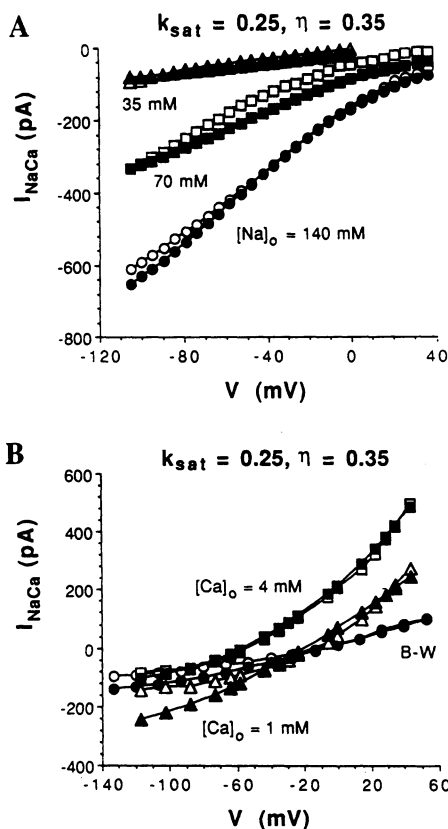


Fig 10. Graphs showing voltage dependence of the Na^+ - Ca^{2+} exchange current (I_{NaCa}) for different values of $[Na^+]$ (A) and for different values of $[Ca^{2+}]_o$ and $[Ca^{2+}]_i$ (B). Solid symbols are simulated values; open symbols are experimental values. Note that the measured⁵³ (Fig 8) dependence of I_{NaCa} on $[Na^+]$ is simulated correctly by the model (A); the conditions are as follows: $[Na^+]$, free, $[Ca^{2+}]_o = 1$ mmol/L, and $[Ca^{2+}]_i = 0.43$ μ mol/L. B demonstrates that the model correctly simulates the voltage dependence of I_{NaCa} for different values of $[Ca^{2+}]_o$ and $[Ca^{2+}]_i$. Note that the experimentally observed property of saturation at very negative potentials is well simulated by the model, except for a deviation for $[Ca^{2+}]_o = 1$ mmol/L. The curves of $[Ca^{2+}]_o = 1$ mmol/L (triangles) and $[Ca^{2+}]_o = 4$ mmol/L (squares) correspond to Fig 9A of Kimura et al.⁵³ The B-W curves (circles) are for $[Ca^{2+}]_o = 2$ mmol/L and correspond to Fig 6B of Beuckelmann and Wier.⁹² Conditions for the simulation in panel B are described in the text. k_{sat} indicates the saturation factor of I_{NaCa} at very negative potentials; η , position of the energy barrier controlling voltage dependence of I_{NaCa} ; and V , membrane potential. Currents shown in the figures are for 0.49 μ F of membrane in panel A, 0.62 μ F of membrane for $[Ca^{2+}]_o = 1$ mmol/L and $[Ca^{2+}]_i = 4$ mmol/L in panel B, and 0.08 μ F of membrane for the B-W curve in panel B. These different membrane areas result from the different cells that were used in the experiments.

μ mol/L in the B-W curve) is also duplicated well by the simulation. Note that the saturation characteristics of $I_{NaCa}(V)$ at very negative potentials are simulated well, except for the curve of $[Ca^{2+}]_o = 1$ mmol/L. This is because I_{NaCa} measured by Kimura et al⁵³ at $[Ca^{2+}]_o = 1$ mmol/L increases slightly at very negative potentials, probably because of contamination by other currents in this potential range. It should be mentioned that $k_{sat} = 0.25$ and $\eta = 0.35$ provide the best fit for these simulations. However, to reconstruct the action potential, $k_{sat} = 0.1$ is used. This is because for the large value ($k_{sat} = 0.25$), the Ca^{2+} -efflux mode of I_{NaCa} is depressed, and Ca^{2+} ions enter the cell through the exchanger. This

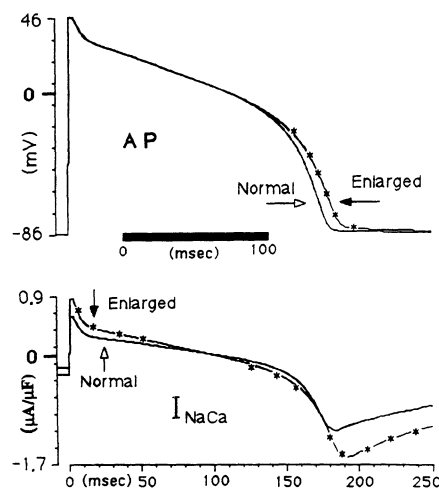


FIG 11. Tracings showing the effects of an augmented Na^+ - Ca^{2+} exchange current (I_{NaCa}) on the action potential (AP). Two APs are superimposed: one is for normal I_{NaCa} (normal conditions); the other is for conditions in which I_{NaCa} is doubled. The only effect of the increase in I_{NaCa} during the late repolarization phase is to prolong the AP duration. The action potential plateau remains unchanged. Currents shown are for $1 \mu\text{F}$ of membrane capacitance.

contradicts the physiological role of I_{NaCa} , which is to extrude Ca^{2+} ions out of the cell. Therefore, $k_{\text{sat}}=0.1$ is used throughout the simulations below. In Fig 11, a simulated action potential is shown (top) for two different strengths of I_{NaCa} , normal and twice the normal amplitude (bottom). The only effect of the increase in I_{NaCa} is to prolong the APD without affecting its plateau potentials. This behavior is consistent with the experimental findings of Doerr et al⁷³ (their Fig 4).

I_V , the Total Time-Independent Current

This current replaces the $I_{\text{K}_{\text{I(T)}}}$ current in the phase-1 model¹ and is the sum of all the time-independent currents, including I_{NaK} , $I_{\text{p(Ca)}}$, $I_{\text{K}_{\text{I}}}$, $I_{\text{K}_{\text{P}}}$, $I_{\text{Ca,b}}$, $I_{\text{Na,b}}$, and $I_{\text{ns(Ca)}}$ (if activated). In Fig 12A, I_V and its components are shown for the range of membrane potentials from -100 to $+50$ mV. Note the major contribution of $I_{\text{K}_{\text{I}}}$ (at $V<0$ mV) and $I_{\text{K}_{\text{P}}}$ (at $V>0$ mV) to I_V . In Fig 12B, current-voltage curves of I_V are shown for four different values of $[\text{K}^+]_o$. Similar to $I_{\text{K}_{\text{I(T)}}}$ of the phase-1 model¹ (their Fig 3) and the experimental findings of Sakmann and Trube⁵² (their Fig 4A), I_V is characterized by a phase of negative slope and a large degree of crossover between the curves for different values of $[\text{K}^+]_o$.

Ionic Currents and Concentration Changes During the Action Potential

In the action potential simulations, \bar{G}_{rel} of the JSR is set to 60 mmol/L per millisecond, which is higher than 18 mmol/L per millisecond used in the square-pulse voltage-clamp simulations that were described in the previous sections. This is because the value of peak I_{Ca} in the action potential simulations is $-6.27 \mu\text{A}/\mu\text{F}$ (Fig 13 below), much lower than the maximum peak I_{Ca} of $-32 \mu\text{A}/\mu\text{F}$ in the square-pulse voltage-clamp simulations. This behavior is in agreement with the experimental findings of Doerr et al,⁷³ who used action potential clamp instead of square-pulse voltage clamp to study the current density of I_{Ca} . Doerr et al found that the

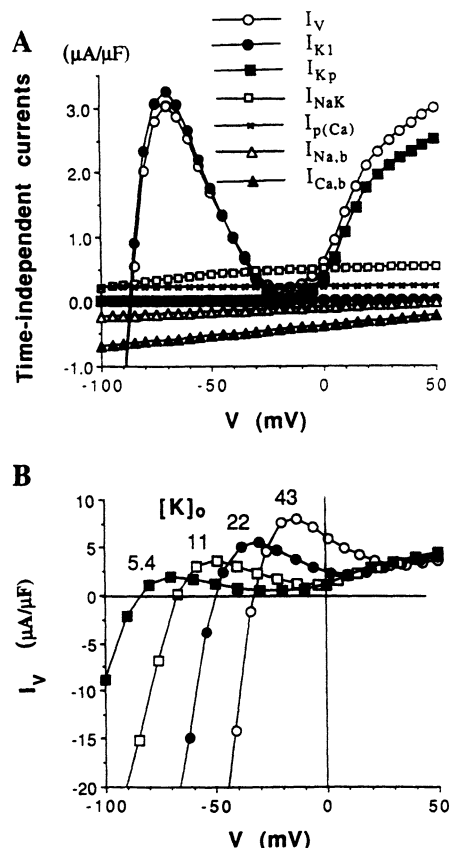


FIG 12. Graphs showing characteristics of the total time-independent current (I_V). A shows the various components of I_V . (See Appendix 2 for definitions of currents.) Note the major contribution of $I_{\text{K}_{\text{I}}}$ for $V<0$ and of $I_{\text{K}_{\text{P}}}$ for $V>0$. I_V displays a phase of negative slope due to a similar property of $I_{\text{K}_{\text{I}}}$. B shows a significant crossover between the current-voltage curves of I_V in response to changes in $[\text{K}^+]_o$. Currents shown are for $1 \mu\text{F}$ of membrane capacitance.

peak current density in their action potential clamp measurements was much lower than the value measured by the square-pulse voltage clamp used by Isenberg and Klöckner³ or by other groups.^{46,88,93} Therefore, in the action potential simulations, to obtain a peak intracellular Ca^{2+} transient of $1.0 \mu\text{mol/L}$ (Fig 5A) with a low peak I_{Ca} , \bar{G}_{rel} had to be increased from 18 to 60 mmol/L per millisecond. This adjustment is consistent with the experimental results of Beuckelmann and Wier,⁴² who found that the peak intracellular Ca^{2+} transient measured by the action potential clamp could reach the same peak value (or even a higher value) than that measured by the square-pulse voltage clamp. This may be because the physiological state of the cell is modified when the square-pulse voltage clamp is applied, affecting the sensitivity of the JSR release channel to changes in $[\text{Ca}^{2+}]_i$.⁹⁴

Figs 13 through 19 depict the simulated time course of the major electrophysiological processes during an action potential. Once the cell is excited by a supra-threshold stimulus, I_{Na} depolarizes the membrane with a maximum rate (\dot{V}_{max}) of 388 V/s to the overshoot potential of 46.5 mV (see Fig 13) and inactivates immediately. Subsequently, I_{Ca} is activated to support the action potential plateau⁹⁵ against the repolarizing currents I_V and I_K . I_{Ca} reaches its peak value of $-6.27 \mu\text{A}/\mu\text{F}$.

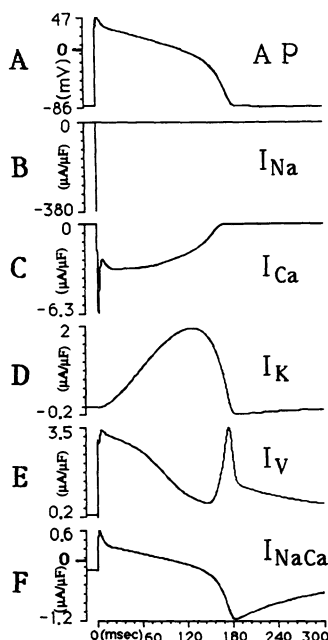


FIG 13. Tracings showing major ionic currents that determine the shape of the action potential (AP). The fast kinetics and large amplitude of the fast Na^+ current (I_{Na} , B) result in the upstroke of the AP (A). The L-type Ca^{2+} current (I_{Ca} , C) is also activated quickly to support the action potential plateau against the repolarizing K^+ current (I_K , D) and the total time-independent current (I_V , E). Finally, the large increase of I_K and the late peak of I_V during its negative slope phase repolarize the membrane to the resting potential. During the late repolarization and early postrepolarization phases, the $\text{Na}^+-\text{Ca}^{2+}$ exchange current (I_{NaCa} , F) is activated to extrude Ca^{2+} ions out of the cell and contributes an additional component of inward current. Currents shown are for 1 μF of membrane capacitance.

$\mu\text{A}/\mu\text{F}$ in 3.23 milliseconds after the onset of stimulation, whereas I_{Na} reaches its (much larger) peak value of $-380 \mu\text{A}/\mu\text{F}$ in 1 millisecond, a time when I_{Ca} is still very small ($-0.97 \mu\text{A}/\mu\text{F}$). Therefore, the early peak of I_{Ca} contributes very little to the rising phase of the action potential. However, the early peak of I_{Ca} determines the cumulative Ca^{2+} entry 2 milliseconds after the onset of V_{max} and, in turn, the release of Ca^{2+} from the JSR and the resulting intracellular Ca^{2+} transient (see below). Finally, the large increase of the delayed I_K together with I_V that operates at its negative slope range (peak I_V at ≈ 180 milliseconds, Fig 13) repolarizes the membrane to the resting potential. In the last panel of Fig 13, I_{NaCa} has almost zero contribution during most of the action potential plateau but is activated during the late plateau and repolarization phases to extrude Ca^{2+} ions out of the cell.⁷⁶ Note that at the late repolarization phase, I_{Ca} is inactivated, but I_{NaCa} is activated and slows down the rate of membrane repolarization.⁷³ The APD is ≈ 180 milliseconds in the measurement range of 207 ± 31 milliseconds⁹⁶ and close to the value of 184.6 milliseconds estimated from the experimental results of Doerr et al.⁷³ Other quantitative measures of the simulated action potential morphology are also consistent with experiments. An average rate of potential change during the plateau is 0.2 V/s (0.3 V/s was estimated from Doerr et al), and during phase-III repolarization, it is 2 V/s (2 V/s was estimated from Doerr et al).

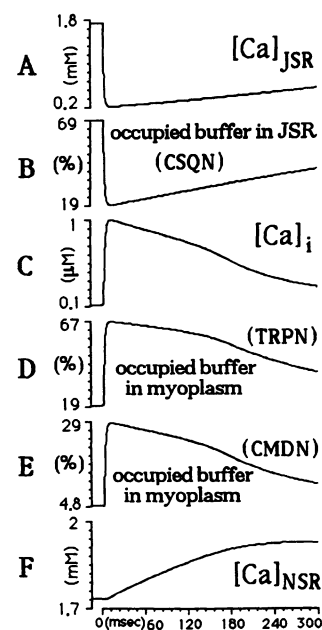


FIG 14. Tracings showing $[\text{Ca}^{2+}]$ changes in the myoplasm and in the sarcoplasmic reticulum (SR) during an action potential. Once it is triggered (at 2 milliseconds), the junctional SR (JSR) releases almost all of its free Ca^{2+} contents (A) and most of the buffered Ca^{2+} (calsequestrin (CSQN), B) into the myoplasm. Of the released Ca^{2+} ions, 97.8% are buffered by troponin (TRPN) and calmodulin (CMDN) in the myoplasm (D and E, respectively), resulting in a peak free $[\text{Ca}^{2+}]_i$ of only 1 $\mu\text{mol/L}$ (C). The released Ca^{2+} ions reenter the network SR (NSR, F) and translocate into JSR. For CSQN, 100% corresponds to buffering of 10 mmol/L of $[\text{Ca}^{2+}]_{JSR}$; for TRPN, 100% corresponds to buffering of 70 $\mu\text{mol/L}$ of $[\text{Ca}^{2+}]_i$; and for CMDN, 100% corresponds to buffering of 50 $\mu\text{mol/L}$ of $[\text{Ca}^{2+}]_i$.

Figs 14 and 15 describe the processes that regulate $[\text{Ca}^{2+}]$ in the cell. In Fig 14, cumulative Ca^{2+} entry of 0.375 $\mu\text{mol/L}$ 2 milliseconds from the onset of V_{max} results in an increase of $[\text{Ca}^{2+}]_i$ from 0.12 $\mu\text{mol/L}$ to only 0.1235 $\mu\text{mol/L}$, which is small due to the buffering of Ca^{2+} in the myoplasm. The Ca^{2+} entry triggers the release of Ca^{2+} ions from the JSR into the myoplasm (Fig 14A and 14B) following the kinetics of the CICR process. The total amount of Ca^{2+} ions released is 6.37 mmol/L (based on the small volume of the JSR), which is equivalent to 45 $\mu\text{mol/L}$ in the large volume of the myoplasm. The value of 6.37 mmol/L released by the JSR is made up of 1.53 mmol/L of free Ca^{2+} and 4.84 mmol/L of Ca^{2+} buffered by CSQN, demonstrating the importance of buffering in the JSR to increase its Ca^{2+} storage capacity. Because of the large capacity buffers in the myoplasm, 97.8% of the released Ca^{2+} ions are buffered (71.7% by troponin and 26.1% by calmodulin), resulting in a peak intracellular Ca^{2+} transient of 1 $\mu\text{mol/L}$ (Fig 14C). These simulated results demonstrate the importance of the myoplasm buffers in maintaining the low level of $[\text{Ca}^{2+}]_i$. Throughout the action potential, Ca^{2+} ions enter the NSR by the uptake process, increasing $[\text{Ca}^{2+}]$ in the NSR from 1.73 to 1.92 $\mu\text{mol/L}$ (Fig 14F). Fig 15 depicts the movement of Ca^{2+} ions inside the cell. As indicated in Fig 15B, the Ca^{2+} ions are released from the JSR into the myoplasm as a spike with a peak rate of 3 mmol/L per millisecond and then reenter the NSR (Fig 15C) with a maximum uptake rate of 2.6 $\mu\text{mol/L}$ per millisecond, which is much greater

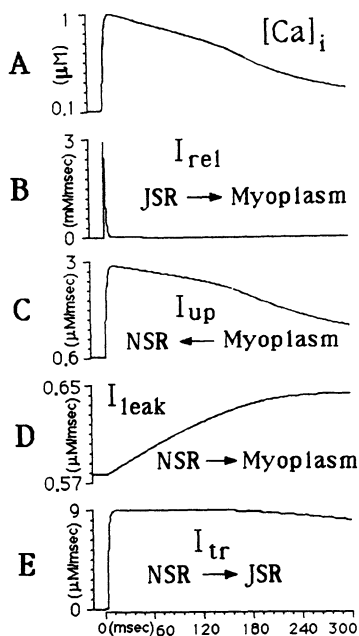


Fig 15. Tracings showing Ca^{2+} fluxes during an action potential. Once the junctional sarcoplasmic reticulum (JSR) is triggered, Ca^{2+} ions are released following impulselike kinetics with a maximum rate of $\approx 3 \text{ mmol/L per millisecond}$ (I_{rel} , B). Then, the Ca^{2+} ions reenter the network sarcoplasmic reticulum (NSR) with a slow uptake rate of $\approx 3 \mu\text{mol/L per millisecond}$ (I_{up} , C). There is also a small leakage of Ca^{2+} from the NSR to the myoplasm at a rate of $0.64 \mu\text{mol/L per millisecond}$ (I_{leak} , D). The translocation of Ca^{2+} from the NSR to the JSR is at a rate of $9 \mu\text{mol/L per millisecond}$ relative to the JSR volume (I_{tr} , E). A shows the $[\text{Ca}^{2+}]_i$ transient during the action potential.

than the maximum leakage rate (Fig 15D) of $0.64 \mu\text{mol/L per millisecond}$, resulting in a net loading of Ca^{2+} ions into the NSR as shown in Fig 14F. Finally, the Ca^{2+} ions that loaded the NSR are translocated into the JSR with a rate of $0.86 \mu\text{mol/L per millisecond}$ (Fig 15E); therefore, the Ca^{2+} content of the JSR increases, as shown in Fig 14A and 14B.

Fig 16 shows the gating processes of the L-type Ca^{2+} channel during an action potential. The d-gate is fully activated at the onset of the action potential upstroke, bringing I_{Ca} to its early peak value of $-6.27 \mu\text{A}/\mu\text{F}$. Then, the increase of $[\text{Ca}^{2+}]_i$ inactivates I_{Ca} through the Ca^{2+} -dependent inactivation process (f_{Ca}) from its peak value to $\approx -3.3 \mu\text{A}/\mu\text{F}$. During the plateau (from 10 to 160 milliseconds), I_{Ca} is determined by the increase in the f_{Ca} -gate (reflecting a decrease in $[\text{Ca}^{2+}]_i$) and a decrease in the f-gate. Finally, during the late repolarization phase, the d-gate is inactivated very early to close the L-type Ca^{2+} channel during this phase. In Fig 17, the ionic currents through the L-type channel are shown. The peak inward current of $I_{\text{Ca},t}$ ($-3.74 \mu\text{A}/\mu\text{F}$) is smaller than that of I_{Ca} ($-6.27 \mu\text{A}/\mu\text{F}$) because of the outward K^+ current, $I_{\text{Ca},\text{K}}$, whose peak value is $3.87 \mu\text{A}/\mu\text{F}$. By using the action potential clamp technique, Doerr et al.⁷³ found that the ratio of peak to plateau Ca^{2+} current is 1.39 ± 0.5 . In the model, this ratio for $I_{\text{Ca},t}$ is 1.28, in the range of the measurements. (Note that $I_{\text{Ca},t}$ is the current measured in the experiments.) There exists a notch in I_{Ca} and $I_{\text{Ca},t}$ (arrows). This is due to the simulated spikelike release of Ca^{2+} from the JSR, resulting in an extremely fast inactivation of I_{Ca} . In the

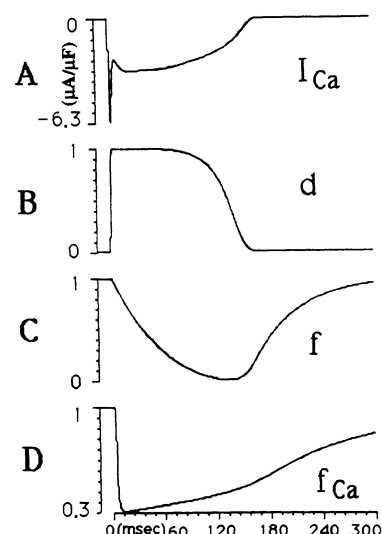


Fig 16. Tracings showing the gating processes of the L-type Ca^{2+} channel. Once the cell is excited, activation parameter d is activated quickly (B) to bring the Ca^{2+} current (I_{Ca}) to its peak value of $-6.27 \mu\text{A}/\mu\text{F}$ within 2 milliseconds (A). The increase of $[\text{Ca}^{2+}]_i$ decreases the I_{Ca} via the Ca^{2+} -dependent inactivation process (f_{Ca} -gate, D). The slow increase of the f_{Ca} -gate (D) and the slow decrease of the inactivation gate (f-gate, C) determine the plateau I_{Ca} . Finally, d is inactivated at the late repolarization phase to close the L-type Ca^{2+} channel. Current shown in panel A is for $1 \mu\text{F}$ of membrane capacitance.

experimental study, a more graded release of Ca^{2+} from the JSR and dispersion of the intracellular Ca^{2+} transient in the cell cause a much smoother inactivation process, eliminating this notch (compare panels A and B of Fig 4).

In Fig 18, six ionic currents that contribute to the total time-independent current, I_v , are shown. Clearly, I_{K_1} and I_{K_p} are the major components of I_v , as described

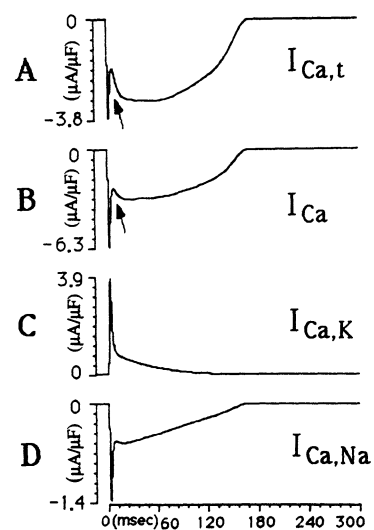


Fig 17. Tracings showing ionic currents through the L-type Ca^{2+} channel. The total current ($I_{\text{Ca},t}$) through this channel is shown (A). The Ca^{2+} current (I_{Ca} , B) and Na^+ current ($I_{\text{Ca},\text{Na}}$, D) are inward currents. The K^+ current ($I_{\text{Ca},\text{K}}$, C) is an outward current, resulting in a peak value of $I_{\text{Ca},t}$ that is smaller than that of I_{Ca} . The arrows in panels A and B indicate a notch in $I_{\text{Ca},t}$ and I_{Ca} , respectively (see text). Currents shown in the figures are for $1 \mu\text{F}$ of membrane capacitance.

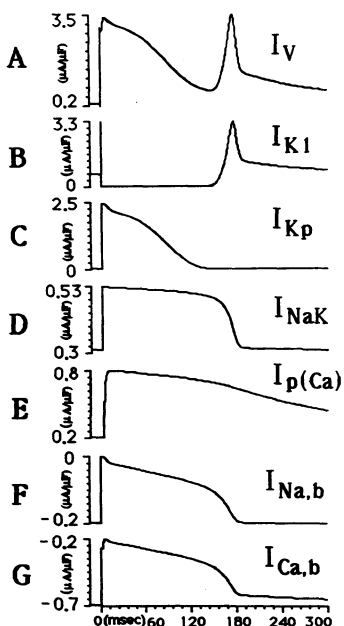


FIG 18. Tracings showing the total time-independent current (I_V) and its components during the action potential. I_V (A) is mostly composed of the time-independent K^+ current (I_{K1} , B) and the plateau K^+ current (I_{Kp} , C); note that each of these currents contributes during a different phase of the action potential. The Na^+ - K^+ pump (I_{NaK} , D) increases during depolarization and pumps Na^+ ions out of the cell throughout the plateau. The Ca^{2+} pump in the sarcolemma ($I_{p(Ca)}$, E) extrudes Ca^{2+} ions from the cell throughout the action potential (in contrast, I_{NaCa} [Fig 19] operates to extrude Ca^{2+} mostly during the late repolarization and early postrepolarization phases). During the action potential plateau, the Na^+ background leakage current ($I_{Na,b}$, F) and the Ca^{2+} background leakage current ($I_{Ca,b}$, G) decrease monotonically because of the decrease of the driving force. Currents shown in the figures are for 1 μF of membrane capacitance.

in the phase-1 model. During the action potential plateau, I_{NaK} (Fig 18D) increases because of the increase of the membrane potential and extrudes Na^+ ions that entered the cell during the upstroke of the action potential. $I_{p(Ca)}$ (Fig 18E) helps I_{NaCa} to extrude Ca^{2+} ions out of the cell. The Na^+ leakage $I_{Na,b}$ and Ca^{2+} leakage $I_{Ca,b}$ (Fig 18F and 18G) both decrease during the action potential plateau because of the decrease of the driving force. In Fig 19, we demonstrate the effect of I_{NaCa} on the peak intracellular Ca^{2+} transient by clamping I_{NaCa} to zero when $I_{NaCa} > 0$ (the results under this condition are marked by asterisks in the figure). As a result, the cumulative Ca^{2+} entry 2 milliseconds from the onset of V_{max} decreases from 0.375 to 0.3 $\mu\text{mol/L}$, and the peak intracellular Ca^{2+} transient also decreases from 1.0 to 0.75 $\mu\text{mol/L}$. Because the smaller peak intracellular Ca^{2+} transient implies a reduced level of Ca^{2+} -dependent inactivation, I_{Ca} is relatively larger, and the plateau potential is more positive.

Discussion

The goal of the present study was to construct a model of the membrane action potential of the mammalian ventricular cell that was based on, whenever possible, recent experimental studies in single-cell and single-channel preparations and in other preparations such as SR vesicles. Individual processes (eg, ionic

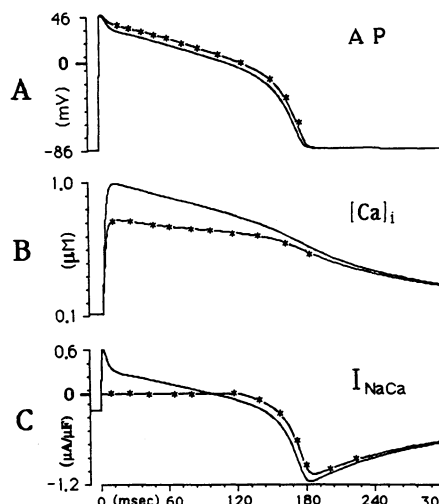


FIG 19. Tracings showing the contribution of the Na^+ - Ca^{2+} exchange current (I_{NaCa}) to the peak intracellular Ca^{2+} transient. The fact that I_{NaCa} (C) is positive during the depolarization phase implies influx of Ca^{2+} ions. This is in addition to the influx of Ca^{2+} through the L-type Ca^{2+} current (I_{Ca}). The resulting larger $[Ca^{2+}]_i$ triggers a larger Ca^{2+} release by the junctional sarcoplasmic reticulum and a greater peak intracellular Ca^{2+} transient (B). The larger $[Ca^{2+}]_i$ causes greater inactivation of I_{Ca} and somewhat decreased plateau action potentials (AP, A). Solid curves indicate the normal operation of I_{NaCa} . For the starred curves, all positive values of I_{NaCa} are set to zero, so I_{NaCa} does not contribute to the Ca^{2+} influx. Currents shown in panel C are for 1 μF of membrane capacitance.

currents) are formulated quantitatively on the basis of experimental data and measured parameter values. The objective was to integrate these components into a model of the cell that could be used to demonstrate possible interactions between these components and to simulate the resulting qualitative cellular behavior. In the first phase of this work,¹ we reformulated five membrane ionic currents: I_{Na} (fast Na^+ inward current), I_K (time-dependent K^+ current), I_{K1} (time-independent K^+ current), I_{Kp} (plateau K^+ current), and I_b (background current). The phase-1 model retained the slow inward current (I_{si}) of the B-R model and was used to investigate physiological phenomena dominated by the Na^+ and K^+ currents listed above. These included effects of changes in $[K^+]_o$ on the action potential and the response of the cell to stimulation and pacing during the late repolarization and early postrepolarization phases of the action potential. The phase-1 model included only ionic currents through gated channels in the sarcolemma. A major limitation of this model was its inability to simulate dynamic changes in ionic concentrations during the action potential. The major thrust of the work presented here (the phase-2 model) was to incorporate such dynamic changes in the model. To do so, we reformulated the Ca^{2+} current through the sarcolemma to be consistent with the most recent experimental findings. We also incorporated currents that are carried across the sarcolemma by processes other than gated ionic channels, ie, pumps and exchangers. Intracellular processes that dynamically regulate $[Ca^{2+}]_i$ were also incorporated in the model. These include Ca^{2+} uptake and release by the SR and buffering of Ca^{2+} in the myoplasm and in the SR. It should be commented that the phase-2 model responded correctly

to all the physiological phenomena investigated by the phase-1 model.

In 1985, DiFrancesco and Noble⁹ developed a dynamic model of the Purkinje action potential, which included many of the processes that were incorporated in the ventricular model presented here. The formulation of the D-N model was limited by the experimental data from single-cell and single-channel studies that were available at the time. Therefore, important properties of the ionic currents and other processes were not incorporated in the D-N model. This was discussed briefly in our previous study.¹ Differences between the D-N Purkinje model and the ventricular model presented here are explored further in the following discussion. In 1990, Rasmusson et al¹⁰ published an action potential model for the frog atrial cell. This model is very different from the ventricular model presented here in that it does not include a representation of the SR and its role in the dynamics of intracellular Ca^{2+} . This is because Ca^{2+} fluxes into or out of the SR are known to be very small in frog atrial cells under normal conditions, and sufficient increase in $[\text{Ca}^{2+}]_i$ to cause contraction can be obtained through I_{Ca} alone. A detailed discussion of the various components of the phase-2 model developed in the present study and of their ability to simulate physiological phenomena is provided below.

I_{Ca} , the Ca^{2+} Current Through the L-Type Ca^{2+} Channel

In the model, only the L-type (long-lasting) Ca^{2+} channel was included. Another type of Ca^{2+} channel exists in cardiac cells and is named the T-type channel ($I_{\text{Ca},T}$) to emphasize its transient properties.⁹⁷ $I_{\text{Ca},T}$ could be clearly identified, but there was only rather weak evidence that this channel might be involved in the regulation of rhythmic activity.⁹⁸ Therefore, it was not incorporated in our model. Compared with the kinetics measured in tissue preparations, the kinetics of the L-type channel measured in single-cell preparations exhibit the following properties: (1) The activation is an order of magnitude faster (the maximum time constant is only 1 or 2 milliseconds as compared with ≈ 40 milliseconds in the B-R model²). (2) The maximum conductance is an order of magnitude larger (0.09 millisiemens in the B-R model but 0.9 millisiemens in our model). (3) Reversal potential and permeability ratios between different ions are much better defined. (4) Inactivation depends not only on the membrane potential but also on $[\text{Ca}^{2+}]_i$. All of these properties are incorporated in the model developed here. The first three observations were made consistently in many experiments in the 1980s; however, the last issue regarding the kinetics of channel inactivation is still controversial since the experimental data are not consistent, as demonstrated in Fig 2. In particular, different characteristics of the voltage-dependent inactivation f-gate were measured in different experiments. We formulated all of these different behaviors (Appendix 3) and used the equations to simulate recent experiments that were conducted in single ventricular cells under normal physiological conditions. The simulations identified a partial-U-shaped f_x and a U-shaped τ_i^{10} as the best choice that correctly duplicates the experimental behavior. This procedure is an example that shows how the model

can be used as a tool for critical evaluation of the conflicting experimental data.

Ca^{2+} Fluxes in the SR

Fabiato³⁰⁻³² suggested functional compartmentation of SR into NSR and JSR but not structural compartmentation. However, in recent experiments, both functional and structural compartmentation of SR could be observed on the basis of these findings: (1) The Ca^{2+} loading rate of the JSR is negligible compared with that of the NSR.²⁷ (2) The loading rate of the JSR is insensitive to ryanodine and ruthenium red, whereas the loading rate of NSR is sensitive to these drugs.²⁹ (3) The Ca^{2+} buffer CSQN exists only in the JSR, not in the NSR; therefore, the density of Ca^{2+} in the JSR is much higher than that in the NSR.²⁸ (4) By use of SR-stained electron micrographs, JSR and NSR can be structurally distinguished but appear contiguous.^{23,24} In our model, SR is compartmentalized both functionally and structurally. NSR, occupying 92% of SR volume, is responsible for Ca^{2+} uptake, whereas JSR, occupying 8% of SR volume, is responsible for Ca^{2+} release. For modeling the release channel of the JSR, we adopt a simple time-dependent process described by an exponential rise and fall.^{78,79} A release model based on the Hodgkin-Huxley type formalism, presented by Wong et al,⁹⁹ is not adopted. This is because (1) its kinetics, obtained from skinned cell preparations, is 100 times slower than that in intact cardiac cells,^{42,79} (2) it does not simulate $[\text{Ca}^{2+}]_i$ wave propagation even when its kinetics is made faster by a factor of 100,⁸⁰ and (3) only functional compartmentation of SR is assumed in their model, and the entire SR, as a single compartment, is responsible for both Ca^{2+} release and uptake.

The amount of Ca^{2+} release in our model depends on the cumulative Ca^{2+} entry into the cell 2 milliseconds from the time of V_{max} or from the time of stimulus.⁴² This accounts for the dependence of Ca^{2+} release on the rate of increase of $[\text{Ca}^{2+}]_i$ observed by Fabiato.³¹ Other properties such as modification of the release channel by H^+ , Na^+ , K^+ , and Mg^{2+} are not incorporated in the model, since there is no evidence that the concentrations of these ions change significantly during the excitation-contraction coupling cycle. The model adequately describes the Ca^{2+} fluxes and concentration changes observed in whole-cell experiments⁴² under normal conditions.

Ca^{2+} Buffers in the Myoplasm and in the JSR

Undoubtedly, without Ca^{2+} buffers in the myoplasm, $[\text{Ca}^{2+}]_i$ cannot be maintained at an appropriate low level (maximum intracellular Ca^{2+} transient of $\approx 1 \mu\text{mol/L}$), and Ca^{2+} ions cannot be loaded appropriately into the NSR when the cell is paced at fast frequencies. As described in "Results," after the initiation of an action potential, $45 \mu\text{mol/L}$ of Ca^{2+} ions were released by the SR into the myoplasm. In the absence of buffers, $[\text{Ca}^{2+}]_i$ would have increased from the resting level of 0.12 to $45.12 \mu\text{mol/L}$ (compared with $1 \mu\text{mol/L}$ in the presence of buffers). This high level of $[\text{Ca}^{2+}]_i$ would have enhanced the Ca^{2+} -efflux mode of I_{NaCa} by a factor of 376 ($=45.12/0.12$). As a result, most of the released Ca^{2+} ions would have been extruded out of the cell during the action potential plateau, resulting in intracellular Ca^{2+} transients that decrease to the resting value during the

plateau phase. In addition, the resulting high negative amplitude of I_{NaCa} would have contributed significantly to the plateau potentials, and I_{NaCa} would have been a major determinant of the action potential plateau. This is the behavior of I_{NaCa} in the D-N model⁹ for Purkinje fibers, in which Ca^{2+} buffers in the myoplasm were not included. A decrease of $[Ca^{2+}]_i$ to the resting value and a major contribution of I_{NaCa} during the action potential plateau are inconsistent with the experimental findings in single ventricular cells.^{42,73,100} For example, Leblanc and Hume¹⁰⁰ found that intracellular Ca^{2+} transients do not decrease or decrease with a very slow rate when the membrane is depolarized in single ventricular cells. Another serious consequence of the absence of buffers is that the cell would have discharged most of its Ca^{2+} content during the action potential plateau because of the enhanced I_{NaCa} . This is completely contradictory to the experimental observation that myocytes can be loaded with Ca^{2+} by pacing. If a paced cell could not be loaded with Ca^{2+} ions, the phenomenon of postextrasystolic inotropic potentiation, found in the experiments, could not be observed.^{79,87} Therefore, without Ca^{2+} buffers in the model, not only is the behavior of I_{NaCa} incorrect, but also, very important physiological phenomena cannot be duplicated by the simulations.

Regarding the Ca^{2+} buffer in the JSR, its role is different from the buffers in the myoplasm. It increases the capacity of the JSR to store Ca^{2+} in a very small volume. The volume of the JSR is only 0.48% of the cell volume, whereas the volume fraction of the myoplasm in the cell is 68%. In the resting state, the free Ca^{2+} content of the JSR is 1.73 mmol/L, which is equivalent to 12.2 μ mol/L in the much larger volume of the myoplasm. If the entire content of free Ca^{2+} in the JSR were released into the myoplasm, $[Ca^{2+}]_i$ could have only reached a level of 0.25 μ mol/L because of the buffering process in the myoplasm. With the [CSQN] buffer in the JSR, 6.84 mmol/L of Ca^{2+} ions are buffered, resulting in a total Ca^{2+} content of 8.57 mmol/L at the resting state. Therefore, the storage capacity of the JSR is increased by a factor of 5 because of the presence of the buffer. This allows the JSR to store sufficient Ca^{2+} ions that on release can bring the peak intracellular Ca^{2+} transient to $\approx 1 \mu$ mol/L and cause muscle contraction.

I_v , the Total Time-Independent Current

The total time-independent current, $I_{K1(T)}$, in the phase-1 model is denoted here as I_v , a time-independent current that depends only on voltage. This is because I_v is not a pure K^+ current and consists of $I_{Na,b}$, $I_{Ca,b}$, $I_{p(Ca)}$, and I_{NaK} in addition to the K^+ currents I_{K1} and I_{Kp} . The protocol for measuring I_v is to apply a slowly changing voltage ramp.⁵² Therefore, the measured I_v definitely includes I_{NaCa} in addition to the six currents listed above. However, the amplitude of I_{NaCa} is greatly affected by intracellular Ca^{2+} transients. This introduces a time-dependent factor into I_v and disturbs its behavior as a purely voltage-dependent current in our simulations. For this reason, we did not include I_{NaCa} in I_v . $I_{p(Ca)}$ and $I_{Ca,b}$ are also dependent on the intracellular Ca^{2+} transient; however, their amplitudes are very small compared with I_{K1} and I_{Kp} , which are the major components of I_v (Fig 18). Therefore, these currents do not introduce a significant time-dependent factor into I_v during the action

potential simulations. It should be mentioned that the $[K^+]_o$ dependence of \bar{G}_{K1} (and therefore of I_v) was not formulated correctly in the D-N model, as we discussed previously.¹ Similar comments apply to the model of Rasmusson et al,¹⁰ since I_{K1} of their model was adopted from the D-N model. Also, both models do not incorporate the plateau K^+ channel, I_{Kp} .

I_{NaK} , the Na^+ - K^+ Pump

The activity of the pump is stimulated by $[K^+]_o$ and $[Na^+]_i$ and is dependent on the membrane potential. The half-saturation concentrations for $[K^+]_o$ and $[Na^+]_i$ have been measured in many experiments,^{62,67-70} whereas the voltage dependence was elucidated only recently by Nakao and Gadsby⁶² and Gadsby and Nakao.²⁵ The voltage-dependence property was not incorporated in the D-N model, and the Gadsby and Nakao data were not used by Rasmusson et al¹⁰ in their formulation, since the data were not published at the time. From the Na^+ ion flux and the time constant of I_{NaK} decay after exposure to zero $[K^+]_o$, Cohen et al⁶⁶ concluded that the Hill coefficient of $[Na^+]_i$ must be >3 . However, all other measurements^{61,68,69} obtain a value <3 . Therefore, a Hill coefficient of 1.5 is used in our model, different from the values 3 and 1 used in the Rasmusson model and in the D-N model, respectively. The formulation simulates correctly the voltage dependence of I_{NaK} for different values of $[Na^+]_o$ (Fig 9).

I_{NaCa} , the Na^+ - Ca^{2+} Exchanger

In recent experiments,^{53,54,92} the properties of $[Na^+]_o$ dependence, $[Ca^{2+}]_o$ dependence, and saturation at very negative potentials of I_{NaCa} were clearly determined. These properties are incorporated in our formulation of I_{NaCa} , which is modified from the formulation in the D-N model. Also, the coefficient $\eta=0.35$ (position of energy barrier) was measured quantitatively after the D-N model was developed and is incorporated in our model.^{53,59,60,92} The new formulation predicts correctly the voltage and ionic concentration dependence of I_{NaCa} as measured in the experiments (Fig 10). This behavior cannot be duplicated by the previous models. Note that the scaling factor, k_{NaCa} , is given in units of current density ($\mu A/\mu F$) and not in the units ($\mu A/[(mmol/L)^4 \cdot \mu F]$) used in the D-N model. Therefore, k_{NaCa} in our model is independent of the ionic concentrations. Also, note that $k_{sat}=0.25$ is used in Fig 10 to simulate the measured property of I_{NaCa} saturation at very negative potentials. However, we found that $k_{sat}=0.25$ depressed the Ca^{2+} -efflux mode of I_{NaCa} so much that I_{NaCa} operated to increase, rather than decrease, $[Ca^{2+}]_i$. The large degree of saturation in the measurements may be caused by the nonphysiological environment of the cells during the experiments. In one set of data measured by Kimura et al⁵³ (ie, the curve of $[Ca^{2+}]_o=1$ mmol/L in Fig 10), the amplitude of I_{NaCa} even decreases slightly at very negative potentials. Therefore, in all simulations except those of Fig 10, a smaller saturation factor ($k_{sat}=0.1$) was used.

$I_{ns(Ca)}$, the Nonspecific Ca^{2+} -Activated Current

This channel was first identified and its properties were measured quantitatively by Ehara et al,⁷¹ who used single-channel recording techniques. In single-cell experiments, a transient inward current (I_{TI}) was observed

under conditions of Ca^{2+} overload. However, it is unclear whether I_{NaCa} alone, $I_{\text{ns(Ca)}}$ alone, or both contribute to I_{Ti} . By measuring the reversal potential of I_{Ti} or using specific blockers for I_{NaCa} , several groups^{72,101} claim that $I_{\text{ns(Ca)}}$ is I_{Ti} , whereas other groups⁵⁹ believe that I_{NaCa} is I_{Ti} . Preliminary simulations using our model suggest that I_{Ti} consists of both I_{NaCa} and $I_{\text{ns(Ca)}}$ and that the relative contribution of these two Ca^{2+} -activated currents to I_{Ti} depends on the conditions. However, this prediction depends on our choice of a value for the maximum conductance of $I_{\text{ns(Ca)}}$. The values provided by Ehara et al.⁷¹ are spread over an order of magnitude (0.036 to 0.36 millisiemens/ μF). Therefore, we determine the maximum conductance on the basis of the effects of $I_{\text{ns(Ca)}}$ on the action potential, measured by Doerr et al.⁷³ With a maximum conductance of 0.072 millisiemens/ μF , our simulated results duplicate the measurements by Doerr et al.⁷³ (Fig 4). This value falls in the range of values suggested by Ehara et al.⁷¹ The ability to narrow down the possible range of conductances to one specific value is essential for a quantitative study of the relative contributions of I_{NaCa} and $I_{\text{ns(Ca)}}$ to I_{Ti} and of their role in arrhythmic activity of the single cell (ie, afterdepolarizations and triggered activity).

I_K , the Time-Dependent (Delayed-Rectifier) K^+ Current

As clarified in "Materials and Methods," the reformulation of I_{Ca} in the model dictated a reformulation of I_K . In the phase-1 model, I_K was formulated to depend on the first power of the activation X-gate, similar to the Beeler and Reuter² formulation (the B-R I_K). In the model presented here, I_K was formulated to depend on X^2 , as suggested by Matsuura et al,⁵¹ on the basis of measurements in the single cell (I_K of Matsuura et al). Comparing the voltage dependence of these two currents, the higher degree of rectification of the B-R \bar{I}_K results in plateau current at high positive potentials that is 4.8 times smaller than that of \bar{I}_K of Matsuura et al. This implies that I_K of Matsuura et al can provide higher repolarizing current and stronger capability of repolarizing the membrane from plateau potentials. As a result, when introduced in the phase-2 model, the B-R I_K fails to repolarize the membrane adequately, and the action potential displays an unrealistically long duration of 400 milliseconds at normal $[K^+]_o = 5.4 \text{ mmol/L}$. In contrast, the large I_K of Matsuura et al at plateau potentials strongly repolarizes the membrane and results in a realistic action potential duration of ≈ 180 milliseconds. It should be noted that these results do not imply that a high degree of rectification is not a correct property of I_K . It may depend on the species and the type of cell. For example, the plateau potential (+17 mV) in the B-R model is smaller than that (+30 mV) in the phase-2 model, and the plateau potentials of Purkinje fibers and atrial cells can be <0 mV. For a low plateau potential, I_K of Matsuura et al becomes smaller than the B-R I_K because of its X^2 kinetics, and the B-R I_K provides more current for repolarizing the membrane. Since the plateau potential of mammalian ventricular cells (except for the rat) is relatively high and positive, I_K of Matsuura et al provides more repolarizing current in these cells. It should be commented that I_K in our model is relatively large and therefore plays a major role in repolarization, which is the case for the guinea pig-type ventricular

cell. For other species, including the rabbit, dog, and rat, I_K is relatively small.

Note that the low degree of rectification of \bar{I}_K of Matsuura et al⁵¹ results in a large degree of crossover between current-voltage curves of different values of $[K^+]_o$ (Fig 8). In contrast, the high degree of rectification of the B-R \bar{I}_K results in a minimal crossover¹ (their Fig 1). It should be noted that the degree of crossover in our model cannot be compared with that predicted by the D-N model or the model of Rasmusson et al,¹⁰ simply because the $[K^+]_o$ dependence of \bar{G}_K is not included in these models. Finally, it should also be mentioned that the characteristics and explanations of mechanisms underlying physiological phenomena simulated by the phase-1 model¹ are independent of whether the B-R I_K or I_K of Matsuura et al is used. This is because supernormality and Wenckebach periodicity result from the interaction between the slow recovery from inactivation of I_{Na} and postrepolarization refractoriness caused by a slow decrease in the X-gate of I_K . This property is shared by both the phase-1 and phase-2 models.

Recently, Sanguinetti and Jurkiewicz¹⁰² have shown that I_K is composed of two overlapping currents, $I_{K,s}$ and $I_{K,r}$. In the present model, we do not separate I_K into its components and maintain its global representation as I_K . This approach is consistent with the focus of the present study, namely, currents and processes that determine intracellular Ca^{2+} and depend on its concentration. The simulations conducted here do not require separation of I_K into $I_{K,s}$ and $I_{K,r}$ and duplicate correctly the global behavior of I_K . In a previous study,¹ we investigated phenomena that involved I_K in a major way, such as supernormal excitability, Wenckebach periodicity, and the effects of changes in $[K^+]_o$. It will be interesting, in future studies, to examine the separate roles and relative importance of $I_{K,s}$ and $I_{K,r}$ in determining these cellular responses.

Electrophysiological Processes During the Action Potential

The time course of ionic currents and concentration changes during an action potential were described in "Results" and depicted in Figs 13 through 19. It is clear from the simulations that in spite of its fast activation (relative to the B-R model), I_{Ca} does not contribute significantly to the rising phase of the action potential. However, the early peak of I_{Ca} is important, since it determines the magnitude of early Ca^{2+} entry into the cell and, in turn, the release of Ca^{2+} from the SR and the intracellular Ca^{2+} transient. It is interesting to note that $[\text{Ca}^{2+}]_i$ inactivates I_{Ca} through the $[\text{Ca}^{2+}]_i$ -dependent inactivation process (f_{Ca} -gate in our formulation). This suggests a negative-feedback control mechanism by which the early I_{Ca} peak influences the inactivation of I_{Ca} . The intracellular Ca^{2+} transient also influences other currents, such as I_{NaCa} and, under certain conditions, $I_{\text{ns(Ca)}}$. The simulations demonstrate the importance of buffering processes in the myoplasm in controlling cellular Ca^{2+} and, therefore, in regulating these currents. A related observation is that I_{NaCa} does not contribute significantly during most of the plateau but influences the rate of membrane repolarization during the repolarization phase and, consequently, the APD. This simulated behavior is in agreement with the experimental observation of Doerr et al.⁷³ An important

limitation of the model is the assumption of intracellular spatial uniformity, especially with regard to the distribution of Ca^{2+} ions. The model assumes a uniform distribution of Ca^{2+} buffers and of the SR. It does not represent restricted diffusion of Ca^{2+} or the spatial distribution of release sites from the JSR. This limitation does not permit the simulation of spatially dependent intracellular phenomena such as " Ca^{2+} waves" and is likely to affect the time course of the Ca^{2+} transient. Representation of these spatial nonuniformities requires detailed knowledge of the spatial distribution of Ca^{2+} buffers and of release and uptake sites in the SR, of the geometry and location of subcellular organelles, of restricted spaces, and of diffusion barriers. Such detailed structural information is not available, and the complexity is beyond our modeling capabilities at present. The implications of the spatial uniformity assumption are discussed further in our accompanying article¹¹ in relation to spontaneous Ca^{2+} release by the SR and the generation of delayed afterdepolarizations.

Summary and Conclusions

In summary, the work presented here is a second phase in the development of an action potential model for mammalian ventricular cells that is based, whenever possible, on recent experimental findings. The model can simulate dynamic changes in ionic concentrations. The emphasis in this study is on ionic currents and other processes that regulate and determine $[\text{Ca}^{2+}]_i$ changes during the action potential. Whereas these processes constitute an important aspect of the electrical activity of the cell and of generating the action potential, they also determine the mechanical activity of the cell through the excitation-contraction coupling process. In our accompanying article,¹¹ we use the model to study a phenomenon that is related to excitation-contraction coupling, namely postextrasystolic mechanical potentiation.^{79,87} Another important aspect of the model is its

ability to simulate spontaneous release of Ca^{2+} from the JSR when the cell is overloaded with Ca^{2+} . This property and the presence of a nonspecific Ca^{2+} -activated current ($I_{\text{ns(Ca)}}$) in the model permit the study of arrhythmic activity related to Ca^{2+} overload, such as afterdepolarizations and triggered activity. These phenomena are also simulated and investigated in the accompanying article. It should be mentioned that several ionic currents were not included in the present model. These include the transient outward current (I_{to}), which will be incorporated in future models once sufficient experimental data become available. Although I_{to} is not observed in guinea pig ventricular cells (of the type modeled here), it is a very important current for repolarization in ventricular cells of other species (eg, dog, rabbit, and rat) and should be included in models of the ventricular action potential in these species. In addition, the T-type Ca^{2+} current ($I_{\text{Ca,T}}$)⁹⁷ and the Cl^- current (I_{Cl})¹⁰³ were not included, since experimental evidence suggests that they play a minimal role under the conditions simulated here (eg, I_{Cl} does not play a significant role in the absence of adrenergic stimulation).¹⁰³ Other channels were not incorporated in the model, since they do not contribute significantly to the processes and phenomena investigated in the present study. These include Ca^{2+} -, ATP-, and Na^+ -activated K^+ currents ($I_{\text{K(Ca)}}$,¹⁰⁴ $I_{\text{K(ATP)}}$,¹⁰⁵ and $I_{\text{K(Na)}}$,¹⁰⁶ respectively). These channels may have to be included in future models for the purpose of studying the effects of ischemia and other abnormalities on the electrical activity of the single cell. We would like to emphasize that the model presented here for the mammalian ventricular action potential is mostly based on the guinea pig ventricular cell. However, it provides the framework for modeling other types of ventricular cells, with appropriate modifications made to account for species differences.

Appendix 1: Formulation of the Model

I. Cell geometry

- a. Dimensions: length (L) = 100 μm ; radius (r) = 11 μm
- b. Cell volume: $V_{\text{cell}} = \pi r^2 L = 38 \times 10^{-6} \mu\text{L}$
- c. Geometric membrane area: $A_{\text{Geo}} = 2\pi r^2 + 2\pi r L = 0.767 \times 10^{-4} \text{ cm}^2$
- d. Capacitive membrane area: $A_{\text{Cap}} = R_{\text{CG}} \cdot A_{\text{Geo}} = 1.534 \times 10^{-4} \text{ cm}^2$
- e. Myoplasm volume: $V_{\text{myo}} = V_{\text{cell}} \cdot 68\% = 25.84 \times 10^{-6} \mu\text{L}$
- f. Mitochondria volume: $V_{\text{mito}} = V_{\text{cell}} \cdot 26\% = 9.88 \times 10^{-6} \mu\text{L}$
- g. SR volume: $V_{\text{SR}} = V_{\text{cell}} \cdot 6\% = 2.28 \times 10^{-6} \mu\text{L}$
- h. NSR volume: $V_{\text{NSR}} = V_{\text{cell}} \cdot 5.52\% = 2.098 \times 10^{-6} \mu\text{L}$
- i. JSR volume: $V_{\text{JSR}} = V_{\text{cell}} \cdot 0.48\% = 0.182 \times 10^{-6} \mu\text{L}$
- j. Cleft volume: $V_{\text{cleft}} = (V_{\text{cell}}/88\%) \cdot 12\% = 5.182 \times 10^{-6} \mu\text{L}$

II. Standard ionic concentrations

$$[\text{K}^+]_o = 5.4 \text{ mmol/L}; [\text{K}^+]_i = 145 \text{ mmol/L}; [\text{Na}^+]_o = 140 \text{ mmol/L}; [\text{Na}^+]_i = 10 \text{ mmol/L}; [\text{Ca}^{2+}]_o = 1.8 \text{ mmol/L}; \text{ and } [\text{Ca}^{2+}]_{i,\text{rest}} = 0.12 \mu\text{mol/L}$$

III. Ionic currents in the sarcolemma

- a. Fast sodium current: I_{Na}
- $I_{\text{Na}} = \bar{G}_{\text{Na}} \cdot m^3 \cdot h \cdot j \cdot (V - E_{\text{Na}});$
- $E_{\text{Na}} = (RT/F) \cdot \ln([{\text{Na}^+}]_o / [{\text{Na}^+}]_i); \text{ and } \bar{G}_{\text{Na}} = 16 \text{ millisiemens}/\mu\text{F}.$

For $V \geq -40$ mV,

$$\alpha_h = \alpha_j = 0.0; \beta_h = 1/\left(0.13\{1+\exp[(V+10.66)/-11.1]\}\right);$$

and $\beta_j = 0.3 \cdot \exp(-2.535 \times 10^{-7}V)/\{1+\exp[-0.1(V+32)]\}$.

For $V < -40$ mV,

$$\alpha_h = 0.135 \cdot \exp[(80+V)/-6.8];$$

$$\beta_h = 3.56 \cdot \exp(0.079V) + 3.1 \times 10^5 \cdot \exp(0.35V);$$

$$\alpha_j = [-1.2714 \times 10^5 \cdot \exp(0.2444V) - 3.474 \times 10^{-5} \cdot \exp(-0.04391V)] \cdot (V+37.78)/\{1+\exp[0.311 \cdot (V+79.23)]\}; \text{ and}$$

$$\beta_j = 0.1212 \cdot \exp(-0.01052V)/\{1+\exp[-0.1378(V+40.14)]\}.$$

And, for all range of V,

$$\alpha_m = 0.32(V+47.13)/\{1-\exp[-0.1(V+47.13)]\};$$

$$\beta_m = 0.08 \cdot \exp(-V/11).$$

b. Currents through the L-type Ca^{2+} channel

$$I_{\text{Ca},t} = I_{\text{Ca}} + I_{\text{Ca,K}} + I_{\text{Ca,Na}};$$

$$I_{\text{Ca}} = d \cdot f \cdot f_{\text{Ca}} \cdot I_{\text{Ca}}; \quad I_{\text{Ca,K}} = d \cdot f \cdot f_{\text{Ca}} \cdot \bar{I}_{\text{Ca,K}}; \quad \text{and } I_{\text{Ca,Na}} = d \cdot f \cdot f_{\text{Ca}} \cdot \bar{I}_{\text{Ca,Na}}.$$

For ion S, including Ca^{2+} , Na^+ , and K^+ ,

$$\bar{I}_S = P_S \cdot z_s^2 \cdot \frac{VF^2 \cdot \gamma_{si} \cdot [S]_i \cdot \exp(z_s VF/RT) - \gamma_{so} \cdot [S]_o}{RT \cdot \exp(z_s VF/RT) - 1};$$

$$P_{\text{Ca}} = 5.4 \times 10^{-4} \text{ cm/s}; \quad \gamma_{\text{Cai}} = 1; \quad \gamma_{\text{Ca}o} = 0.341;$$

$$P_{\text{Na}} = 6.75 \times 10^{-7} \text{ cm/s}; \quad \gamma_{\text{Nai}} = \gamma_{\text{Na}o} = 0.75;$$

$$P_K = 1.93 \times 10^{-7} \text{ cm/s}; \quad \gamma_{\text{Ki}} = \gamma_{\text{Ko}} = 0.75;$$

$$f_{\text{Ca}} = 1/[1+([Ca^{2+}]_i/K_{m,\text{Ca}})^2]; \quad K_{m,\text{Ca}} = 0.6 \text{ } \mu\text{mol/L};$$

$$d_s = 1/\{1+\exp[-(V+10)/6.24]\};$$

$$\tau_d = d_s \cdot \{1-\exp[-(V+10)/6.24]\}/[0.035 \cdot (V+10)];$$

$$f_s = 1/[1+\exp[(V+35.06)/8.6]] + 0.6/[1+\exp[(50-V)/20]]; \quad$$

$$\tau_f = 1/\left(0.0197 \cdot \exp\{-[0.0337 \cdot (V+10)]^2\} + 0.02\right);$$

$$\alpha_d = d_s/\tau_d; \quad \beta_d = (1-d_s)/\tau_d; \quad \alpha_f = f_s/\tau_f; \quad \text{and } \beta_f = (1-f_s)/\tau_f.$$

c. Time-dependent K^+ current: I_K

$$I_K = \bar{G}_K \cdot X_i \cdot X^2 \cdot (V - E_K); \quad P_{\text{Na},K} = 0.01833;$$

$$E_K = (RT/F) \cdot \ln\{([K^+]_o + P_{\text{Na},K}[Na^+]_o)/([K^+]_i + P_{\text{Na},K}[Na^+]_i)\};$$

$$\bar{G}_K = 0.282 \cdot \sqrt{[K^+]_o}/5.4 \text{ millisiemens}/\mu\text{F};$$

$$X_i = 1/[1+\exp[(V-56.26)/32.1]];$$

$$\alpha_x = 7.19 \times 10^{-5} \cdot (V+30)/\{1-\exp[-0.148 \cdot (V+30)]\}; \text{ and}$$

$$\beta_X = 1.31 \times 10^{-4} \cdot (V+30)/\{-1+\exp[0.0687 \cdot (V+30)]\}.$$

d. Time-independent K^+ current: I_{K1}

$$I_{K1} = \bar{G}_{K1} \cdot K_{1,i} \cdot (V - E_{K1}); \quad E_{K1} = (RT/F) \cdot \ln([K^+]_o/[K^+]_i);$$

$$\bar{G}_{K1} = 0.75 \cdot \sqrt{[K^+]_o}/5.4 \text{ millisiemens}/\mu\text{F};$$

$$\alpha_{K1} = 1.02/\{1+\exp[0.2385 \cdot (V - E_{K1} - 59.215)]\}; \text{ and}$$

$$\beta_{K1} = \{0.49124 \cdot \exp[0.08032 \cdot (V - E_{K1} + 5.476)] + \exp[0.06175 \cdot (V - E_{K1} - 594.31)]\}/\{1+\exp[-0.5143 \cdot (V - E_{K1} + 4.753)]\}.$$

e. Plateau K^+ current: I_{Kp}

$$I_{Kp} = \bar{G}_{Kp} \cdot K_p \cdot (V - E_{Kp}); \quad \bar{G}_{Kp} = 0.0183 \text{ millisiemens}/\mu\text{F};$$

$$E_{Kp} = E_{K1}; \quad \text{and } K_p = 1/[1+\exp[(7.488-V)/5.98]].$$

f. Na^+ - Ca^{2+} exchanger: I_{NaCa}

$$I_{\text{NaCa}} = k_{\text{NaCa}} \cdot \frac{1}{K_{m,\text{Na}}^3 + [Na^+]_o^3} \cdot \frac{1}{K_{m,\text{Ca}} + [Ca^{2+}]_o} \cdot \frac{1}{1 + k_{\text{sat}} \cdot \exp\left[(\eta-1) \cdot V \cdot \frac{F}{RT}\right]}$$

$$\cdot \{\exp\left(\eta \cdot V \cdot \frac{F}{RT}\right) [Na^+]_i^3 \cdot [Ca^{2+}]_o - \exp\left[(\eta-1) \cdot V \cdot \frac{F}{RT}\right] [Na^+]_o^3 \cdot [Ca^{2+}]_i\};$$

$$k_{\text{NaCa}} = 2000 \text{ } \mu\text{A}/\mu\text{F}; \quad K_{m,\text{Na}} = 87.5 \text{ mmol/L}; \quad K_{m,\text{Ca}} = 1.38 \text{ mmol/L}; \quad k_{\text{sat}} = 0.1; \quad \text{and } \eta = 0.35.$$

g. Na^+ - K^+ pump: I_{NaK}

$$I_{\text{NaK}} = \bar{I}_{\text{NaK}} \cdot f_{\text{NaK}} \cdot \frac{1}{1 + (K_{m,\text{Na}i}/[Na^+]_i)^{1.5}} \cdot \frac{[K^+]_o}{[K^+]_o + K_{m,\text{Ko}}};$$

$$\bar{I}_{NaK} = 1.5 \mu\text{A}/\mu\text{F}; \quad K_{m,Na} = 10 \text{ mmol/L}; \quad K_{m,Ko} = 1.5 \text{ mmol/L};$$

$$f_{NaK} = \frac{1}{1 + 0.1245 \cdot \exp\left(-0.1 \cdot \frac{VF}{RT}\right) + 0.0365 \cdot \sigma \cdot \exp\left(-\frac{VF}{RT}\right)}; \text{ and}$$

$$\sigma = \frac{1}{7} \cdot \left[\exp\left(\frac{[Na^+]_o}{67.3}\right) - 1 \right].$$

h. Nonspecific Ca^{2+} -activated current: $I_{ns(Ca)}$

$$I_{ns,K} = \bar{I}_{ns,K} \cdot \frac{1}{1 + (K_{m,ns(Ca)} / [Ca^{2+}]_i)^3};$$

$$I_{ns,Na} = \bar{I}_{ns,Na} \cdot \frac{1}{1 + (K_{m,ns(Ca)} / [Ca^{2+}]_i)^3};$$

$$I_{ns(Ca)} = I_{ns,K} + I_{ns,Na};$$

$$P_{ns(Ca)} = 1.75 \cdot 10^{-7} \text{ cm/s}; \quad K_{m,ns(Ca)} = 1.2 \mu\text{mol/L}; \text{ and}$$

$$E_{ns(Ca)} = \frac{RT}{F} \cdot \ln \frac{[K^+]_o + [Na^+]_o}{[K^+]_i + [Na^+]_i}.$$

(\bar{I}_{ns} is computed from P_{ns} using the relation in IIIb of this appendix with the same γ values.)

i. Sarcolemmal Ca^{2+} pump: $I_{p(Ca)}$

$$I_{p(Ca)} = \bar{I}_{p(Ca)} \cdot \frac{[Ca^{2+}]_i}{K_{m,p(Ca)} + [Ca^{2+}]_i};$$

$$\bar{I}_{p(Ca)} = 1.15 \mu\text{A}/\mu\text{F}; \quad K_{m,p(Ca)} = 0.5 \mu\text{mol/L}.$$

j. Ca^{2+} background current: $I_{Ca,b}$

$$I_{Ca,b} = \bar{G}_{Ca,b} \cdot (V - E_{Ca,N});$$

$$E_{Ca,N} = (RT/2F) \cdot \ln([Ca^{2+}]_o / [Ca^{2+}]_i); \quad \text{and } \bar{G}_{Ca,b} = 0.003016 \text{ millisiemens}/\mu\text{F}.$$

k. Na^+ background current: $I_{Na,b}$

$$I_{Na,b} = \bar{G}_{Na,b} \cdot (V - E_{Na,N}); \quad E_{Na,N} = E_{Na}; \quad \text{and } \bar{G}_{Na,b} = 0.00141 \text{ millisiemens}/\mu\text{F}.$$

l. Total time-independent current: I_V

$$I_V = I_{K1} + I_{Kp} + I_{p(Ca)} + I_{Na,b} + I_{Ca,b} + I_{NaK}.$$

IV. Ca^{2+} buffers in the myoplasm

Troponin (TRPN) and calmodulin (CMDN);

$$\text{buffered } [TRPN] = [\overline{TRPN}] \cdot \{[Ca^{2+}]_i / ([Ca^{2+}]_i + K_{m,TRPN})\};$$

$$\text{buffered } [CMDN] = [\overline{CMDN}] \cdot \{[Ca^{2+}]_i / ([Ca^{2+}]_i + K_{m,CMDN})\};$$

$$[\overline{TRPN}] = 70 \mu\text{mol/L}; \quad [\overline{CMDN}] = 50 \mu\text{mol/L}; \quad K_{m,TRPN} = 0.5 \mu\text{mol/L}; \quad \text{and } K_{m,CMDN} = 2.38 \mu\text{mol/L}.$$

V. Ca^{2+} fluxes in the sarcoplasmic reticulum

a. Ca^{2+} -induced Ca^{2+} release of JSR

$$I_{rel} = G_{rel} \cdot ([Ca^{2+}]_{JSR} - [Ca^{2+}]) \text{ mmol/L per millisecond}$$

If $\Delta[Ca^{2+}]_{i,2} > \Delta[Ca^{2+}]_{i,th}$ 2 milliseconds after the time of V_{max} ,

$$G_{rel} = \bar{G}_{rel} \cdot \frac{\Delta[Ca^{2+}]_{i,2} - \Delta[Ca^{2+}]_{i,th}}{K_{m,rel} + \Delta[Ca^{2+}]_{i,2} - \Delta[Ca^{2+}]_{i,th}} \cdot (1 - \exp[-t/\tau_{on}]) \cdot \exp[-t/\tau_{off}];$$

$$\Delta[Ca^{2+}]_{i,th} = 0.18 \mu\text{mol/L}; \quad K_{m,rel} = 0.8 \mu\text{mol/L}; \quad \tau_{on} = \tau_{off} = 2 \text{ milliseconds}; \quad t = 0 \text{ at time of CICR};$$

$\bar{G}_{rel} = 18 \text{ ms}^{-1}$ for voltage clamp simulations; and

$\bar{G}_{rel} = 60 \text{ ms}^{-1}$ for action potential simulations.

If $\Delta[Ca^{2+}]_{i,2} < \Delta[Ca^{2+}]_{i,th}$ at 2 milliseconds, $\bar{G}_{rel} = 0$.

b. Ca^{2+} release of JSR under Ca^{2+} -overload conditions

$$I_{rel} = G_{rel} \cdot ([Ca^{2+}]_{JSR} - [Ca^{2+}]) \text{ mmol/L per millisecond}$$

If buffered $[CSQN] \geq [CSQN]_{th}$,

$$G_{rel} = \bar{G}_{rel} \cdot (1 - \exp[-t/\tau_{on}]) \cdot \exp[-t/\tau_{off}];$$

$$G_{rel} = 4 \text{ ms}^{-1}; \quad [CSQN]_{th} = 0.7 \text{ or higher}; \quad \text{and } \tau_{on} = \tau_{off} = 2 \text{ milliseconds}; \quad \text{and } t = 0 \text{ at time of spontaneous release.}$$

If buffered $[CQSN] < [CQSN]_{th}$, $\bar{G}_{rel} = 0$.

c. Ca^{2+} buffer in JSR and CSQN

$$\text{Buffered } [CSQN] = [\overline{CSQN}] \cdot \{[Ca^{2+}]_{JSR} / ([Ca^{2+}]_{JSR} + K_{m,CSQN})\}; \quad [\overline{CSQN}] = 10 \text{ mmol/L}; \quad \text{and } K_{m,CSQN} = 0.8 \text{ mmol/L}.$$

- d. Ca^{2+} uptake and leakage of NSR: I_{up} and I_{leak}
 $I_{\text{up}} = I_{\text{up}} \cdot [\text{Ca}^{2+}] / ([\text{Ca}^{2+}] + K_{m,\text{up}})$ mmol/L per millisecond; $I_{\text{leak}} = K_{\text{leak}} \cdot [\text{Ca}^{2+}]_{\text{NSR}}$ mmol/L per millisecond;
 $K_{m,\text{up}} = 0.92 \mu\text{mol/L}$; $I_{\text{up}} = 0.005 \text{ mmol/L per millisecond}$;
 $K_{\text{leak}} = \bar{I}_{\text{up}} / [\text{Ca}^{2+}]_{\text{NSR}} \text{ ms}^{-1}$; and $[\text{Ca}^{2+}]_{\text{NSR}} = 15 \text{ mmol/L}$.
- e. Translocation of Ca^{2+} ions from NSR to JSR: I_{tr}
 $I_{\text{tr}} = ([\text{Ca}^{2+}]_{\text{NSR}} - [\text{Ca}^{2+}]_{\text{JSR}}) / \tau_{\text{tr}}$ mmol/L per millisecond; $\tau_{\text{tr}} = 180 \text{ milliseconds}$.

Appendix 2: Definition of Symbols

- I_{Na} : fast Na^+ current, $\mu\text{A}/\mu\text{F}$
- I_K : time-dependent K^+ current, $\mu\text{A}/\mu\text{F}$
- \bar{I}_K : fully activated K^+ current ($\bar{I}_K = I_K/X$), $\mu\text{A}/\mu\text{F}$
- I_{Ca} : Ca^{2+} current through the L-type Ca^{2+} channel, $\mu\text{A}/\mu\text{F}$
- $I_{\text{Ca},\text{Na}}$: Na^+ current through the L-type Ca^{2+} channel, $\mu\text{A}/\mu\text{F}$
- $I_{\text{Ca},\text{K}}$: K^+ current through the L-type Ca^{2+} channel, $\mu\text{A}/\mu\text{F}$
- $I_{\text{Ca},t}$: total current through the L-type Ca^{2+} channel ($I_{\text{Ca},t} = I_{\text{Ca}} + I_{\text{Ca},\text{Na}} + I_{\text{Ca},\text{K}}$), $\mu\text{A}/\mu\text{F}$
- I_{Kl} : time-independent K^+ current, $\mu\text{A}/\mu\text{F}$
- I_{Kp} : plateau K^+ current, $\mu\text{A}/\mu\text{F}$
- I_{NaCa} : Na^+ - Ca^{2+} exchanger, $\mu\text{A}/\mu\text{F}$
- k_{NaCa} : scaling factor of I_{NaCa} , $\mu\text{A}/\mu\text{F}$
- k_{sat} : saturation factor of I_{NaCa} at very negative potentials
- η : position of the energy barrier controlling voltage dependence of I_{NaCa}
- I_{NaK} : Na^+ - K^+ pump, $\mu\text{A}/\mu\text{F}$
- f_{NaK} : voltage-dependence parameter of I_{NaK}
- σ : $[\text{Na}^+]_o$ -dependence factor of f_{NaK}
- $I_{p(\text{Ca})}$: Ca^{2+} pump in the sarcolemma, $\mu\text{A}/\mu\text{F}$
- $I_{\text{ns},\text{Na}}$: Na^+ current through the nonspecific Ca^{2+} -activated channel, $\mu\text{A}/\mu\text{F}$
- $I_{\text{ns},\text{K}}$: K^+ current through the nonspecific Ca^{2+} -activated channel, $\mu\text{A}/\mu\text{F}$
- $I_{\text{ns}(\text{Ca})}$: nonspecific Ca^{2+} -activated current ($I_{\text{ns}(\text{Ca})} = I_{\text{ns},\text{Na}} + I_{\text{ns},\text{K}}$), $\mu\text{A}/\mu\text{F}$
- $I_{\text{Ca},b}$: Ca^{2+} background leakage current, $\mu\text{A}/\mu\text{F}$
- $I_{\text{Na},b}$: Na^+ background leakage current, $\mu\text{A}/\mu\text{F}$
- I_V : total time-independent current ($I_V = I_{\text{Kl}} + I_{\text{Kp}} + I_{p(\text{Ca})} + I_{\text{Na},b} + I_{\text{Ca},b} + I_{\text{NaK}}$), $\mu\text{A}/\mu\text{F}$
- I_{rel} : Ca^{2+} release from JSR to myoplasm, mmol/L per millisecond
- G_{rel} : rate constant of Ca^{2+} release from JSR, ms^{-1}
- \bar{G}_{rel} : maximum rate constant of Ca^{2+} release from JSR, ms^{-1}
- $\Delta[\text{Ca}^{2+}]_{i,2}$: cumulative Ca^{2+} entry into the cell 2 milliseconds after onset of stimulus or \dot{V}_{max} , $\mu\text{mol/L}$
- $\Delta[\text{Ca}^{2+}]_{i,\text{th}}$: threshold for external triggering of Ca^{2+} release from JSR, $\mu\text{mol/L}$
- τ_{on} and τ_{off} : time constants of activating (on) and deactivating (off) Ca^{2+} release from JSR, milliseconds
- $[\text{CSQN}]_{\text{th}}$: threshold of Ca^{2+} -bound [CSQN] for internal triggering of Ca^{2+} release from JSR under Ca^{2+} -overload conditions
- I_{up} : Ca^{2+} uptake from myoplasm to NSR, mmol/L per millisecond
- I_{leak} : Ca^{2+} leakage from NSR to myoplasm, mmol/L per millisecond
- K_{leak} : rate constant of Ca^{2+} leakage from NSR, ms^{-1}
- I_{tr} : Ca^{2+} transfer from NSR to JSR, mmol/L per millisecond
- τ_{tr} : time constant of Ca^{2+} transfer from NSR to JSR, milliseconds
- \bar{I}_i : maximum current through channel i , $\mu\text{A}/\mu\text{F}$
- \bar{G}_i : maximum conductance of channel i , millisiemens/ μF
- m , h , and j : activation gate, fast inactivation gate, and slow inactivation gate of I_{Na} , respectively
- d and f : activation gate and (voltage-dependent) inactivation gate, respectively, of the L-type Ca^{2+} channel
- f_{Ca} : Ca^{2+} -dependent inactivation gate of the L-type Ca^{2+} channel
- X and X_i : activation gate and inactivation gate of I_K , respectively
- $K1$: inactivation gate of I_{Kl}

y_s : steady-state value of activation (inactivation) gate y
 α_y and β_y : opening and closing rate constants of gate y, respectively, ms⁻¹
 τ_y : time constant of gate y, milliseconds
 $[A]$: maximum concentration of ion A, mmol/L
 V_C : volume of compartment C, μL
 F_C : cellular volume fraction of compartment C
 C_m : total cellular membrane capacitance, μF
 C_{sc} : specific membrane capacity, equal to 1 $\mu\text{F}/\mu\text{F}$
 A_{Geo} : geometric membrane area, cm²
 A_{Cap} : capacitive membrane area ($=C_m/C_{sc}$), cm²
 R_{CG} : ratio of A_{Cap} to A_{Geo}
CSQN: calsequestrin, Ca²⁺ buffer in JSR
TRPN: troponin, Ca²⁺ buffer in the myoplasm
CMDN: calmodulin, Ca²⁺ buffer in the myoplasm
 $K_{m,i}$: half-saturation concentration of channel i, mmol/L
V: membrane potential, mV
 \dot{V} : time derivative of V, mV/ms
 \dot{V}_{max} : maximum rate of rise of V, mV/ms
 P_A : permeability of membrane to ion A, cm/s
 $P_{A,B}$: permeability ratio of ion A to ion B
 E_A : reversal potential of ion A, mV
 $E_{A,N}$: Nernst potential of ion A, mV
 γ_A : activity coefficient of ion A
 z_A : valence of ion A
 $[A]_o$ and $[A]_i$: extracellular and intracellular concentrations of ion A, respectively, mmol/L
F: Faraday constant, 96 500 coulombs/mol
R: gas constant, 1.987 calories/mol/°K
T: absolute temperature, °K
 Q_{10} : temperature adjustment factor, $A(T=t1)=A(T=t2) \cdot (Q_{10})^{(t2-t1)/10}$

Appendix 3. Alternative Formulations of f

- Conventional f_s ; Kass and Sanguinetti τ_f :

$$f_s = 1/\{1+\exp[(V+30)/8]\};$$

$$\tau_f = 16.88 + 462.46 \cdot C_1/(1.0 + C_2);$$

$$C_1 = \exp[0.092 \cdot (V+21.68)]; \text{ and } C_2 = \exp[0.246 \cdot (V+21.68)].$$
- Hadley and Hume f_s ; Kass and Sanguinetti τ_f :

$$f_s = 0.59/\{1.0 + \exp[0.059 \cdot (V+26.12)]\} + 0.41;$$

$$\tau_f = 16.88 + 462.46 \cdot C_1/(1.0 + C_2);$$

$$C_1 = \exp[0.092 \cdot (V+21.68)]; \text{ and } C_2 = \exp[0.246 \cdot (V+21.68)].$$
- Rasmusson et al:

$$f_s = 1/\{1+\exp[(V+35.06)/8.6]\} + 0.6/\{1+\exp[(50-V)/20]\};$$

$$\tau_f = 1/\left(0.0197 \cdot \exp\{-[0.0337 \cdot (V+10)]^2\} + 0.02\right).$$
- D-N model:

$$\alpha_d = 0.03 \cdot (V+24)/\{1-\exp[-(V+24)/4]\};$$

$$\beta_d = 0.012 \cdot (V+24)/\{-1+\exp[(V+24)/10]\};$$

$$\alpha_f = 0.00625 \cdot (V+34)/\{-1+\exp[(V+34)/4]\}; \text{ and}$$

$$\beta_f = 0.05/\{1+\exp[-(V+34)/4]\};$$

$$\alpha_t = f_s/\tau_f; \text{ and } \beta_t = (1-f_s)/\tau_f.$$

Acknowledgments

This study was supported by grants HL-49054 and HL-33343 from the National Heart, Lung, and Blood Institute, National Institutes of Health, and by a grant from the National Science Council, Republic of China (NSC 82-0404-E-006-412). Special thanks to Jinglin Zeng, Robin Shaw, and Xiaoqin Zou for their help with the revision of this article. We also thank Weilun Quan for helpful discussions. We acknowledge the use of facilities at the National Cheng Kung University in Taiwan, Republic of China.

References

- Luo CH, Rudy Y. A model of the ventricular cardiac action potential, depolarization, repolarization, and their interaction. *Circ Res*. 1991;68:1501-1526.
- Beeler GW, Reuter H. Reconstruction of the action potential of ventricular myocardial fibres. *J Physiol (Lond)*. 1977;268:177-210.
- Isenberg G, Klöckner U. Calcium currents of isolated bovine ventricular myocytes are fast and of large amplitude. *Pflugers Arch*. 1982;395:30-41.
- Josephson IR, Sanchez-Chapula J, Brown AM. A comparison of calcium currents in rat and guinea pig single ventricular cells. *Circ Res*. 1984;54:144-156.
- Kass RS, Sanguineti MC. Inactivation of calcium channel current in the calf cardiac Purkinje fiber: evidence for voltage- and calcium-mediated mechanisms. *J Gen Physiol*. 1984;84:705-726.
- Lee KS, Marban E, Tsien RW. Inactivation of calcium channels in mammalian heart cells: joint dependence on membrane potential and intracellular calcium. *J Physiol (Lond)*. 1985;364:395-411.
- Hess P, Lansman JB, Tsien RW. Calcium channel selectivity for divalent and monovalent cations, voltage and concentration dependence of single channel current in ventricular heart cells. *J Gen Physiol*. 1986;88:293-319.
- Hadley RW, Hume JR. An intrinsic potential-dependent inactivation mechanism associated with calcium channels in guinea-pig myocytes. *J Physiol (Lond)*. 1987;389:205-222.
- DiFrancesco D, Noble D. A model of cardiac electrical activity incorporating ionic pumps and concentration changes. *Philos Trans R Soc Lond Biol*. 1985;307:353-398.
- Rasmusson RL, Clark JW, Giles WR, Robinson K, Clark RB, Shibata EF, Campbell DL. A mathematical model of electrophysiological activity in a bullfrog atrial cell. *Am J Physiol*. 1990;259:H370-H389.
- Luo C-H, Rudy Y. A dynamic model of the cardiac ventricular action potential, II: afterdepolarizations, triggered activity, and potentiation. *Circ Res*. 1994;74:1097-1113.
- Rudy Y, Quan W. A model study of the effects of the discrete cellular structure on electrical propagation in cardiac tissue. *Circ Res*. 1987;61:815-823.
- Rudy Y, Quan W. Propagation delays across gap junctions and their reflection in extracellular potentials: a simulation study. *J Cardiovasc Electrophysiol*. 1991;2:299-315.
- Quan W, Rudy Y. Unidirectional block and reentry of cardiac excitation: a model study. *Circ Res*. 1990;66:367-382.
- Hodgkin AL, Huxley AF. A quantitative description of membrane current and its application to conduction and excitation in nerve. *J Physiol (Lond)*. 1952;117:500-544.
- Rush S, Larsen H. A particular algorithm for solving dynamic membrane equations. *IEEE Trans Biomed Eng*. 1978;25:389-392.
- Victorri B, Vinet A, Robege FA, Drouhard JP. Numerical integration in the reconstruction of cardiac action potentials using Hodgkin-Huxley-type models. *Comput Biomed Res*. 1985;18:10-23.
- Dennis JE, Gay DM, Welsch RE. An adaptive nonlinear least-squares algorithm. *ACM Trans Math Software*. 1981;7:348-368.
- Weidmann S. Electrical constants of trabecular muscle from mammalian heart. *J Physiol (Lond)*. 1970;210:1041-1054.
- Isenberg G, Klöckner U. Calcium tolerant ventricular myocytes prepared by preincubation in a "KB medium." *Pflugers Arch*. 1982;395:6-18.
- Hume JR, Uehara A. Ionic basis of the different action potential configurations of single guinea-pig atrial and ventricular myocytes. *J Physiol (Lond)*. 1985;368:525-544.
- Giles WR, Imaizumi Y. Comparison of potassium currents in rabbit atrial and ventricular cells. *J Physiol (Lond)*. 1988;405:123-145.
- Forbes MS, Hawkey LA, Jirge SK, Sperelakis N. The sarcoplasmic reticulum of mouse heart, its divisions, configurations, and distribution. *J Ultrastruct Res*. 1985;93:1-16.
- Forbes MS, Sperelakis N. Ultrastructure of mammalian cardiac muscle. In: Sperelakis N, ed. *Physiology and Pathophysiology of the Heart*. 2nd ed. Boston, Mass: Kluwer Academic Publishers; 1989:3-41.
- Gadsby DC, Nakao M. Steady-state current-voltage relationship of the Na/K pump in guinea pig ventricular myocytes. *J Gen Physiol*. 1989;94:511-537.
- Mathias RT, Eisenberg B, Datyner NB, Cohen IS. Impedance and morphology of isolated canine cardiac Purkinje myocytes: comparison with intact strand preparations. *Biophys J*. 1985;47:49a. Abstract.
- Inui M, Wang S, Saito A, Fleischer S. Characterization of junctional and longitudinal sarcoplasmic reticulum from heart muscle. *J Biol Chem*. 1988;263:10843-10850.
- Jorgensen AO, Broderick R, Somlyo AP, Somlyo AV. Two structurally distinct calcium storage sites in rat cardiac sarcoplasmic reticulum: an electron microprobe analysis study. *Circ Res*. 1988;63:1060-1069.
- Rardon DP, Cefali DC, Mitchell RD, Seiler SM, Jones LR. High molecular weight proteins purified from cardiac junctional sarcoplasmic reticulum vesicles are ryanodine-sensitive calcium channels. *Circ Res*. 1989;64:779-789.
- Fabiato A. Rapid ionic modifications during the aequorin-detected calcium transient in a skinned canine cardiac Purkinje cell. *J Gen Physiol*. 1985;85:189-246.
- Fabiato A. Time and calcium dependence of activation and inactivation of calcium-induced release of calcium from the sarcoplasmic reticulum of a skinned canine cardiac Purkinje cell. *J Gen Physiol*. 1985;85:247-289.
- Fabiato A. Simulated calcium current can both cause calcium loading in and trigger calcium release from the sarcoplasmic reticulum of a skinned canine cardiac Purkinje cell. *J Gen Physiol*. 1985;85:291-320.
- Stern MD, Capogrossi MC, Lakatta EG. Spontaneous calcium release from the sarcoplasmic reticulum in myocardial cells, mechanisms and consequences. *Cell Calcium*. 1988;9:247-256.
- Gerdes AM, Kasten FH. Morphometric study of endomyocardium and epicardium of the left ventricle in adult dogs. *Am J Anat*. 1980;159:389-394.
- Severs NJ, Slade AM, Powell T, Twist VW, Jones GE. Morphometric analysis of the isolated calcium-tolerant cardiac myocyte. *Cell Tissue Res*. 1985;240:159-168.
- Schaper J, Meiser E, Stammel G. Ultrastructural morphometric analysis of myocardium from dogs, rats, hamsters, mice, and from human hearts. *Circ Res*. 1985;56:377-391.
- Blatter LA, McGuigan JA, Reverdin EC. Sodium/calcium exchange and calcium buffering in mammalian ventricular muscle. *Jpn Heart J*. 1986;27(suppl 1):93-107.
- Sheu S-S, Fozard HA. Transmembrane Na^+ and Ca^{2+} electrochemical gradients in cardiac muscle and their relationship to force development. *J Gen Physiol*. 1982;80:325-351.
- Cannell MB, Berlin JR, Lederer WJ. Effects of membrane potential changes on the calcium transient in single rat cardiac muscle cells. *Science*. 1987;238:1419-1423.
- Abete P, Vassalle M. Relation between Na^+-K^+ pump, Na^+ activity and force in strophanthidin inotropy in sheep cardiac Purkinje fibres. *J Physiol (Lond)*. 1988;404:275-299.
- Takamatsu T, Wier WG. Calcium waves in mammalian heart, quantification of origin, magnitude, waveform, and velocity. *FASEB J*. 1990;4:1519-1525.
- Beuckelmann DJ, Wier WG. Mechanism of release of calcium from sarcoplasmic reticulum of guinea-pig cardiac cells. *J Physiol (Lond)*. 1988;405:233-255.
- Drouhard JP, Robege FA. Revised formulation of the Hodgkin-Huxley representation of the sodium current in cardiac cells. *Comput Biomed Res*. 1987;20:333-350.
- Ebihara L, Johnson EA. Fast sodium current in cardiac muscle: a quantitative description. *Biophys J*. 1980;32:779-790.
- Campbell DL, Giles WR, Hume JR, Noble D, Shibata EF. Reversal potential of calcium currents in bull-frog atrial myocytes. *J Physiol (Lond)*. 1988;403:267-286.
- Cavalie A, McDonald TF, Pelzer D, Trautwein W. Temperature-induced transitory and steady-state changes in the calcium current of guinea pig ventricular myocytes. *Pflugers Arch*. 1985;405:294-296.

47. Standen NB, Stanfield PR. A binding-site model for calcium channel inactivation that depends on calcium entry. *Proc R Soc Lond Biol.* 1982;217:101-110.
48. Markwardt F, Nilius B. Modulation of calcium channel currents in guinea-pig single ventricular heart cells by the dihydropyridine BAY K8644. *J Physiol (Lond).* 1988;399:559-575.
49. Campbell DL, Giles WR, Hume JR, Shibata EF. Inactivation of calcium currents in bull-frog atrial myocytes. *J Physiol (Lond).* 1988;403:287-315.
50. Yue DT, Backx PH, Imredy JP. Calcium-sensitive inactivation in the gating of single calcium channels. *Science.* 1990;250: 1735-1738.
51. Matsuura H, Ehara T, Imoto Y. An analysis of the delayed outward current in single ventricular cells of the guinea pig. *Pflugers Arch.* 1987;410:596-603.
52. Sakmann B, Trube G. Conductance properties of single inwardly rectifying potassium channels in ventricular cells from guinea-pig heart. *J Physiol (Lond).* 1984;347:641-657.
53. Kimura J, Miyamae S, Noma A. Identification of sodium-calcium exchange current in single ventricular cells of guinea-pig. *J Physiol (Lond).* 1987;384:199-222.
54. Ehara T, Matsuoka S, Noma A. Measurement of reversal potential of Na-Ca exchange current in single guinea-pig ventricular cells. *J Physiol (Lond).* 1989;410:227-249.
55. Bridge JHB, Smolley JR, Spitzer KW. The relationship between charge movements associated with I_{Ca} and I_{NaCa} in cardiac myocytes. *Science.* 1990;248:376-378.
56. Wier WG, Beuckelmann DJ. Sodium-calcium exchange in mammalian heart: current-voltage relation and intracellular calcium concentration. *J Mol Cell Biochem.* 1989;89:97-102.
57. Yasui K, Kimura J. Is potassium co-transported by the cardiac Na-Ca exchanger? *Pflugers Arch.* 1990;415:513-515.
58. Mullins LJ. A mechanism for Na/Ca transport. *J Gen Physiol.* 1977;70:681-695.
59. Lipp P, Pott L. Transient inward current in guinea-pig atrial myocytes reflects a change of sodium-calcium exchange current. *J Physiol (Lond).* 1988;397:601-630.
60. Lagnado L, McNaughton PA. Electrogenic properties of the Na, Ca exchange. *J Membr Biol.* 1990;113:177-191.
61. Gadsby DC. The Na/K pump of cardiac myocytes. In: Zipes D, Jalife J, eds. *Cardiac Electrophysiology—From Cell to Bedside.* Philadelphia, Pa: WB Saunders Co; 1990:35-51.
62. Nakao M, Gadsby DC. [Na] and [K] dependence of the Na/K pump current-voltage relationship in guinea-pig ventricular myocytes. *J Gen Physiol.* 1989;94:539-565.
63. Daut J, Rudel R. The electrogenic sodium pump in guinea-pig ventricular muscle: inhibition of pump current by cardiac glycosides. *J Physiol (Lond).* 1982;330:243-264.
64. Daut J. Inhibition of the sodium pump in guinea-pig ventricular muscle by dihydroouabain: effects of external potassium and sodium. *J Physiol (Lond).* 1983;339:643-662.
65. Daut J. The energetics of the Na, K-pump in cardiac muscle. In: *Fortschritte der Zoologie, Luttgau (Hrsg): Volume 33, Membrane Control.* Stuttgart/New York: Gustav Fischer Verlag; 1986: 419-427.
66. Cohen IS, Kline RP, Pennefather P, Mulrine NK. Models of Na-K pump in cardiac muscle predict the wrong intracellular Na^+ activity. *Proc R Soc Lond Biol.* 1987;231:371-382.
67. Cohen IS, Datyner NB, Gintant GA, Mulrine NK, Pennefather P. Properties of an electrogenic sodium-potassium pump in isolated canine Purkinje myocytes. *J Physiol (Lond).* 1987;383:251-267.
68. Sejersted OM, Wasserstrom JA, Fozard HA. Na,K pump stimulation by intracellular Na in isolated, intact sheep cardiac Purkinje fibers. *J Gen Physiol.* 1988;91:445-466.
69. Mogul DJ, Singer DH, Ten Eick RE. Dependence of Na-K pump current on internal Na^+ in mammalian cardiac myocytes. *Am J Physiol.* 1990;259:H488-H496.
70. Stimers JR, Shigeto N, Lieberman M. Na/K pump current in aggregates of cultured chick cardiac myocytes. *J Gen Physiol.* 1990;95:61-76.
71. Ehara T, Noma A, Ono K. Calcium-activated non-selective cation channel in ventricular cells isolated from adult guinea-pig hearts. *J Physiol (Lond).* 1988;403:117-133.
72. Cannell MB, Lederer WJ. The arrhythmogenic current I_{TP} in the absence of electrogenic sodium-calcium exchange in sheep cardiac Purkinje fibres. *J Physiol (Lond).* 1986;374:201-219.
73. Doerr T, Denger R, Doerr A, Trautwein W. Ionic currents contributing to the action potential in single ventricular myocytes of the guinea pig studied with action potential clamp. *Pflugers Arch.* 1990;416:230-237.
74. Caroni P, Zurini M, Clark A, Carafoli E. Further characterization and reconstitution of the purified Ca-pumping ATPase of heart sarcolemma. *J Biol Chem.* 1983;258:7305-7310.
75. Hilgemann DW, Noble D. Excitation-contraction coupling and extracellular calcium transients in rabbit atrium: reconstruction of basic cellular mechanisms. *Proc R Soc Lond Biol.* 1987;230: 163-205.
76. Campbell DL, Giles WR, Robinson K, Shibata EF. Studies of the sodium-calcium exchanger in bull-frog atrial myocytes. *J Physiol (Lond).* 1988;403:317-340.
77. Robertson SP, Johnson JD, Potter JD. The time-course of Ca^{2+} exchange with calmodulin, troponin, parvalbumin, and myosin in response to transient increases in Ca^{2+} . *Biophys J.* 1987;34: 559-569.
78. Cannell MB, Allen DG. Model of calcium movements during activation in the sarcomere of frog skeletal muscle. *Biophys J.* 1984;45:913-925.
79. Wier WG, Yue DT. Intracellular calcium transients underlying the short-term force-interval relationship in ferret ventricular myocardium. *J Physiol (Lond).* 1986;376:507-530.
80. Backx PH, de Tombe PP, Van Deem JHK, Mulder BJM, ter Keurs HEDJ. A model of propagating calcium-induced calcium release mediated by calcium diffusion. *J Gen Physiol.* 1989;93: 963-977.
81. Kawano S, Lee CJ, Coronado R. Ca^{2+} dependent activation and inactivation of Ca^{2+} release channels in the sarcoplasmic reticulum of cardiac and skeletal muscle. *J Mol Cell Cardiol.* 1990;22(suppl 1):P90. Abstract.
82. Chamberlain BK, Volpe P, Fleischer S. Calcium-induced calcium release from purified cardiac sarcoplasmic reticulum vesicles. *J Biol Chem.* 1984;259:7540-7546.
83. Mulder BJM, de Tombe PP, ter Keurs HEDJ. Spontaneous and propagated contractions in rat cardiac trabeculae. *J Gen Physiol.* 1989;93:943-961.
84. Capogrossi MC, Stern MD, Spurgeon HA, Lakatta EG. Spontaneous Ca^{2+} release from the sarcoplasmic reticulum limits Ca^{2+} -dependent twitch potentiation in individual cardiac myocytes: a mechanism for maximum inotropy in the myocardium. *J Gen Physiol.* 1988;91:133-155.
85. Haynes DH, Mandveno A. Computer modeling of Ca^{2+} pump function of Ca^{2+} - Mg^{2+} -ATPase of sarcoplasmic reticulum. *Physiol Rev.* 1987;67:244-284.
86. Tada M, Shigekawa M, Kadoma M, Nimura Y. Uptake of calcium by sarcoplasmic reticulum and its regulation and functional consequences. In: Sprelaklis N, ed. *Physiology and Pathophysiology of the Heart.* 2nd ed. Boston, Mass: Kluwer Academic Publishers; 1989:267-290.
87. Yue DT, Burkhoff D, Franz MR, Hunter WC, Sagawa K. Post-extrasystolic potentiation of the isolated canine left ventricle: relationship to mechanical restitution. *Circ Res.* 1985;56:340-350.
88. McDonald TF, Cavalie A, Trautwein W, Pelzer D. Voltage-dependent properties of macroscopic and elementary calcium channel currents in guinea pig ventricular myocytes. *Pflugers Arch.* 1986;406:437-448.
89. Kamp TJ, Sanguineti MC, Miller RJ. Voltage- and use-dependent modulation of cardiac calcium channels by the dihydropyridine (+)-202-791. *Circ Res.* 1989;64:338-351.
90. Gettes LS, Reuter H. Slow recovery from inactivation of inward currents in mammalian myocardial fibres. *J Physiol (Lond).* 1974; 240:703-724.
91. Robinson RB, Boyden PA, Hoffman BF, Hewett KW. Electrical restitution process in dispersed canine cardiac Purkinje and ventricular cells. *Am J Physiol.* 1987;253:H1018-H1025.
92. Beuckelmann DJ, Wier WG. Sodium-calcium exchange in guinea-pig cardiac cells, exchange current and changes in intracellular Ca^{2+} . *J Physiol (Lond).* 1989;414:499-520.
93. Malecot CO, Trautwein W. On the relationship between \dot{V}_{max} of slow responses and Ca-current availability in whole-cell clamped guinea pig heart cells. *Pflugers Arch.* 1987;410:15-22.
94. Meissner G, Henderson JS. Rapid calcium release from cardiac sarcoplasmic reticulum vesicles is dependent on Ca^{2+} and is modulated by Mg^{2+} , adenine nucleotide, and calmodulin. *J Biol Chem.* 1987;262:3065-3073.
95. Campbell DL, Giles WR, Shibata EF. Ion transfer characteristics of the calcium current in bull-frog atrial myocytes. *J Physiol (Lond).* 1988;403:239-266.
96. Priori SG, Corr PB. Mechanisms underlying early and delayed afterdepolarizations induced by catecholamines. *Am J Physiol.* 1990;258:H1796-H1805.

97. Pelzer D, Cavalie A, McDonald TF, Trautwein W. Calcium channels in single heart cells. In: Piper HM, Isenberg G, eds. *Isolated Adult Cardiomyocytes*. Boca Raton, Fla: CRC Press Inc; 1989;2:29-73.
98. Droogmans G, Nilius B. Kinetic properties of the cardiac T-type calcium channel in the guinea-pig. *J Physiol (Lond)*. 1989;419: 627-650.
99. Wong AYK, Fabiato A, Bassingthwaite JB. Model of Ca release mechanism from the sarcoplasmic reticulum: Ca-mediated activation, inactivation and reactivation. In: Sideman S, Beyar R, eds. *Activation, Metabolism and Perfusion of the Heart*. Dordrecht, The Netherlands: Martinus Nijhoff Publishers; 1987: 281-295.
100. Leblanc N, Hume JR. Sodium current-induced release of calcium from cardiac sarcoplasmic reticulum. *Science*. 1990;248: 372-376.
101. Giles WR, Shimoni Y. Comparison of sodium-calcium exchanger and transient inward currents in single cells from rabbit ventricle. *J Physiol (Lond)*. 1989;417:465-481.
102. Sanguinetti MC, Jurkiewicz NK. Delayed rectifier outward K⁺ current is composed of two currents in guinea pig atrial cells. *Am J Physiol*. 1991;260:H393-H399.
103. Harvey RD, Clark CD, Hume JR. Chloride current in mammalian cardiac myocytes. *J Gen Physiol*. 1990;95:1077-1102.
104. Tohse N. Calcium-sensitive delayed rectifier potassium current in guinea pig ventricular cells. *Am J Physiol*. 1990;258:H1200-H1207.
105. Horie M, Irisawa H, Noma A. Voltage-dependent magnesium block of adenosine-triphosphate-sensitive potassium channel in guinea-pig ventricular cells. *J Physiol (Lond)*. 1987;387:251-272.
106. Luk H-N, Carmeliet E. Na⁺-activated K⁺ current in cardiac cells, rectification, open probability, block and role in digitalis toxicity. *Pflugers Arch*. 1990;416:766-768.